Developing new pharmacological tools to modulate transposable elements' activity in colorectal cancer

Amanda Mendes da Silva

Thesis submitted to the University of Ottawa
in partial fulfillment of the requirements for the
Master of Science degree in
Cellular and Molecular Medicine

Department of Cellular and Molecular Medicine
Faculty of Medicine
University of Ottawa

© Amanda Mendes da Silva, Ottawa, Canada, 2023

Acknowledgment

Firstly, I would like to express my deepest gratitude to Dr. Yannick Benoit, without whom this project would not have been possible. I greatly appreciate all the guidance, knowledge, and support offered during this journey. Thank you for providing me with the opportunity to evolve as a better scientist, for entrusting me with the freedom to explore and learn throughout the process, and for fostering a spirit of teamwork in the lab. The lessons I have learned will undoubtedly shape my entire professional trajectory.

I am also thankful to my advisory committee members, Dr. Ryan Russell and Dr. Derrick Gibbings, for their scientific discussions and words of encouragement that have paved the way for the success of my research aims. Furthermore, I would like to thank Dr. Russell and Dr. David Lohnes for evaluating my thesis and participating in my thesis defense.

Thanks, should also go to the members of the Cell Biology and Image Acquisition (CBIA) core facility, and the Louise Pelletier Histology core facility for their invaluable assistance in preparing and imaging samples.

I would like to extend my sincere thanks to Chris Bergin for his unwavering guidance, and scientific advice, and for constantly encouraging me to step outside my comfort zone. Your support and friendship made my graduate studies much more enjoyable. To my fellow lab members Josh, Tanguy, Tamara, Muhammad, and Veronika, I am truly grateful for your help with experiments, engaging in critical discussions, providing feedback, and offering moral support.

I also want to acknowledge all my friends, especially Ana Claudia, for her unwavering support. Despite the physical distance, you remained my source of encouragement, guiding me through the daily challenges of life as a graduate student.

Finally, I want to express my heartful appreciation to my wonderful parents, Marcia Mendes, and Daniel Silva, who taught me the importance of facing new challenges with resilience and pursuing my goals relentlessly. Thanks to my sister Julia and my brother Hugo for their support and belief in me throughout this process. Importantly, I am immensely grateful to James, who never stopped believing in me, encouraging me, and bringing laughter and relaxation to even the most stressful days. Lastly, thanks to my Canadian family, Tracey, Rick, and Catherine, who have shown me unconditional love since 2013 when I first came here, and who promptly embraced my journey as a graduate student, contributing to the completion of this degree.

To all of you, my eternal appreciation.

Table of Contents

List of Figures

List of Tables

List of Abbreviations

5AZA	5-Azacitidine
5-FU	5-Fluorouracil
BME	Basement membrane extract
CCSC	Colorectal cancer stem cell
CMS	Consensus molecular subtypes
CRC	Colorectal cancer
CSC	Cancer stem cell
DHE	Dihydroergotamine
DNA	Deoxy-ribonucleic acid
DNMT	DNA methyltransferase
dsRNA	Double-stranded RNA
GSEA	Gene set enrichment analysis
GTC	Global tissue consenting
H3	Histone 3
H3K27me3	Histone-3, lysine-27 trimethylation
H3K9me2	Histone-3, lysine-9 dimethylation
H3K9me3	Histone-3, lysine-9 trimethylation
ISG	Interferon-stimulated genes
IFN	Interferon
L1ORF1p	LINE-1 open reading frame 1 protein
L1ORF2p	LINE-1 open reading frame 2 protein

LINE-1	Long interspersed nuclear element 1
OCT4	Octamer-binding transcription factor 4
RNA	Ribonucleic Acid
RBP	RNA-binding protein
RNP	Ribonucleoprotein particle
RTi	Reverse transcriptase inhibitor
SINE	Small interspersed nuclear elements
t-hESC	Transformed-human embryonic stem cells
TE	Transposable element
UBR	Ubrogepant
VXN	Vanoxerine

Abstract

LINE-1 retrotransposons, also known as “jumping genes”, are repetitive sequences capable of copying, pasting, and reinserting themselves into the genome. These events were documented at high frequency in various types of cancers, including colorectal cancer (CRC). Furthermore, the expression of proteins encoded by these elements, such as L1ORF1p, has been linked to cancer aggressiveness, stemness, and lower patient survival rates.

Colorectal cancer stem cells (CCSC), constitute a small subset of cells endowed with pluripotency and self-renewal abilities. They play roles in tumorigenesis, cancer aggressiveness, drug resistance, cancer recurrence, and metastasis. Conventional chemotherapeutics primarily target bulk tumor cells and tend to spare cancer stem cell populations. Consequently, targeting CCSC is expected to significantly increase complete remission and survival rates in CRC patients. Here, I have characterized specific aspects of a novel repurposed drug that effectively targets CCSC, reactivates the expression of transposable elements and, consequently, triggers an innate immune response. Further, I tested an *in silico* drug screening approach to identify compounds with high predicted affinity for the RNA binding domains of L1ORF1p, a key protein for the LINE1 retrotransposition event to occur, from a virtual drug library. Two lead compounds, both FDA-approved drugs, were identified and evaluated for their capacity to block L1ORF1p nuclear translocation, a needed step to complete the LINE1 lifecycle, as well as their capacity to decrease LINE-1 retrotransposition levels.

In addition, I established a protocol for the isolation, culture, propagation, and cryopreservation of patient-derived normal colonic organoids. This protocol is crucial to the establishment of a colonic organoid biobank, representing a powerful resource to assess cancer-

selective toxicity of putative CCSC-targeting compounds. Together, this thesis emphasizes the importance of transposable elements in CRC and contributes to the establishment of a gold standard *ex vivo* disease-modeling system for the discovery of new therapeutic agents.

Introduction

1.1 Colorectal cancer

Colorectal Cancer (CRC) is a highly prevalent disease in the world. In Canada, CRC is the second leading cause of death from cancer in men and the third leading cause of death from cancer in women [1]. It is estimated that the number of young patients diagnosed with CRC is increasing globally and is anticipated to become the leading cause of cancer death in individuals aged 20 to 49 in the United States by 2030 [2]. This type of malignancy poses a significant threat, especially given that approximately 50% of CRC patients who undergo treatment may later experience metastasis or relapse [3]. Therefore, there is an urgent need to understand the mechanisms behind tumorigenesis, cancer progression, and acquired therapeutic resistance to develop novel therapeutic strategies and reduce the high death rates associated with CRC.

Colorectal carcinoma typically emerges in three patterns: sporadic, inherited, or familial. Sporadic diseases make up around 70% to 75% of cases [4]. Genetically, sporadic CRCs develop through the accumulation of a series of anomalies in tumor suppressor genes and oncogenes. The majority of colorectal cancers have their origins in benign adenomas, which are small growths of tissue inside the colon or rectum lumen, forming adenomatous polyps. These polyps may contain abnormal crypts and have the potential to evolve into carcinomas [4-6]. This transformation into malignancy is thought to be a gradual process, taking about 5-10 years, during which mutations and epigenetic changes accumulate [5, 7]. Nonetheless, the progression can occur more rapidly in certain patients.

Currently, three primary molecular classifications for CRC have been proposed. The chromosomal instability (CIN) pathway involves generating gene deletions, duplications, and

rearrangements in chromosomes. This type of genomic instability is the most prevalent, appearing in 70-85% of CRCs, mainly in tumors proficient in DNA mismatch repair (MMR) [8]. Another significant pathway is the microsatellite instability (MSI) pathway, which arises due to deficiencies in DNA MMR and is marked by frequent mutations at simple nucleotide repeat sequences. MSI is present in about 15% of sporadic CRC cases [9]. The third pathway termed the CpG island methylator phenotype (CIMP) pathway, is recognized by widespread CpG island methylation. This form of epigenetic instability influences the development of CRC [10-12]. Although one form of genomic/epigenomic instability generally takes precedence in the progression of a specific CRC, MSI and CIMP often coexist [13].

Recently, a systematic analysis has introduced a structured method called the consensus molecular subtypes (CMS) to describe the genetic and molecular mutations discovered in CRC [14]. This innovative CMS approach enables the categorization of CRC patients into four distinct molecular subtypes determined by an extensive analysis of their transcriptional genomes. Briefly, CMS1 has MSI and mutations in CIMP and BRAF pathways. CMS2 can be identified by mutations in specific pathways linked to cellular metabolism. CMS3 has a KRAS mutation as a hallmark. CMS4 exhibits mutations in pathways related to fibrogenesis and mesenchymal-epithelial transition, which are associated with a worse prognosis. The classification offered by CMS can be a significant advancement in providing answers such as the use of adjuvant chemotherapy in stage II, personalized first-line chemotherapy for metastatic CRC, and potentially identifying new targeted therapies that address specific pathways within each distinct molecular subtype [14].

In the clinic, CRC is categorized by the TNM system, based on the size of the tumor (T), lymph node invasion (N), and tumor infiltration to a different part of the body (M; metastasis) [15]. This system provides valuable prognostic information, such as guidance for therapy decisions

and estimation of the 5-year survival rate. Briefly, the tumor is classified from stage 0 to IV, stage 0, I, and II being treated mainly by surgical resection. Radiotherapy is almost always advised while chemotherapy may be used before or after surgery, whereas stage III includes tumors that have invaded lymph nodes near the colon or rectum, and surgery is the main treatment. Chemoradiation combines chemotherapy and radiotherapy and is usually given before surgery, as 25 to 30 treatments of radiation with 5-fluorouracil (5-FU) or capecitabine over 5 to 6 weeks. When chemotherapy is given alone after surgery, several drug combinations could be chosen such as FOLFOX (folinic acid + 5-FU + oxaliplatin), CAPOX (capecitabine + oxaliplatin), FOLFIRI (folinic acid + 5-FU + irinotecan), and others. Finally, stage IV is when the tumor has spread to distant organs or lymph nodes (metastasis) and treatments are used depending on if the cancer can be removed with surgery (resectable) or not (unresectable). Aside from tumor resection, patients are normally treated with chemotherapy alone or with a combination of chemotherapy, radiotherapy, targeted therapy, and/or immunotherapy. The therapy regimen and the order they are used depend on whether the cancer can be removed with surgery or not (unresectable) [16]. Recurrent cancer means that the tumor has come back after it has been treated and is treated as stage IV cancer (**Figure 1**).

Despite numerous treatments available for CRC, survival rates can differ tremendously depending on the stage of the tumor. According to the American Cancer Society, the overall 5-year relative survival rate for all stages of colorectal cancer is around 65% [17]. However, that rate varies from 90% for patients diagnosed with early-stage CRC while patients in late stages have their 5-year survival rate dropped to 11% [18]. Importantly, the emergence of immunotherapy and the development of immune checkpoint inhibitors represent a significant advance in the treatment of specific malignancies, such as non-small cell lung carcinoma, melanoma, and refractory

Hodgkin's lymphoma [19]. However, in CRC, the clinical benefits from immune checkpoint inhibitors were mainly observed in patients presenting high MSI and/or MMR deficiency, which represents only 15-20% of clinical cases. Thus, a vast majority of CRC cases are non-responders facing such a therapeutic approach [19, 20]. Conventional therapies successfully target the bulk of the tumor, but they often fail to eradicate subpopulations of highly tumorigenic cells, leading to high rates of drug resistance, cancer recurrence, and metastasis [21, 22]. A relationship between cancer stemness and tumor immunogenicity was recently established, where the presence of CSCs would repel cytotoxic T cells from infiltrating tumor mass and promote immune evasion [23, 24]. Ultimately, developing new strategies to target this specific subgroup of cells represents an opportunity to either promote lymphocytic infiltration in the tumor microenvironment or boost response to immune checkpoint inhibitors, potentially improving the chances of complete eradication of cancer and consequently enhancing survival rates of CRC patients.

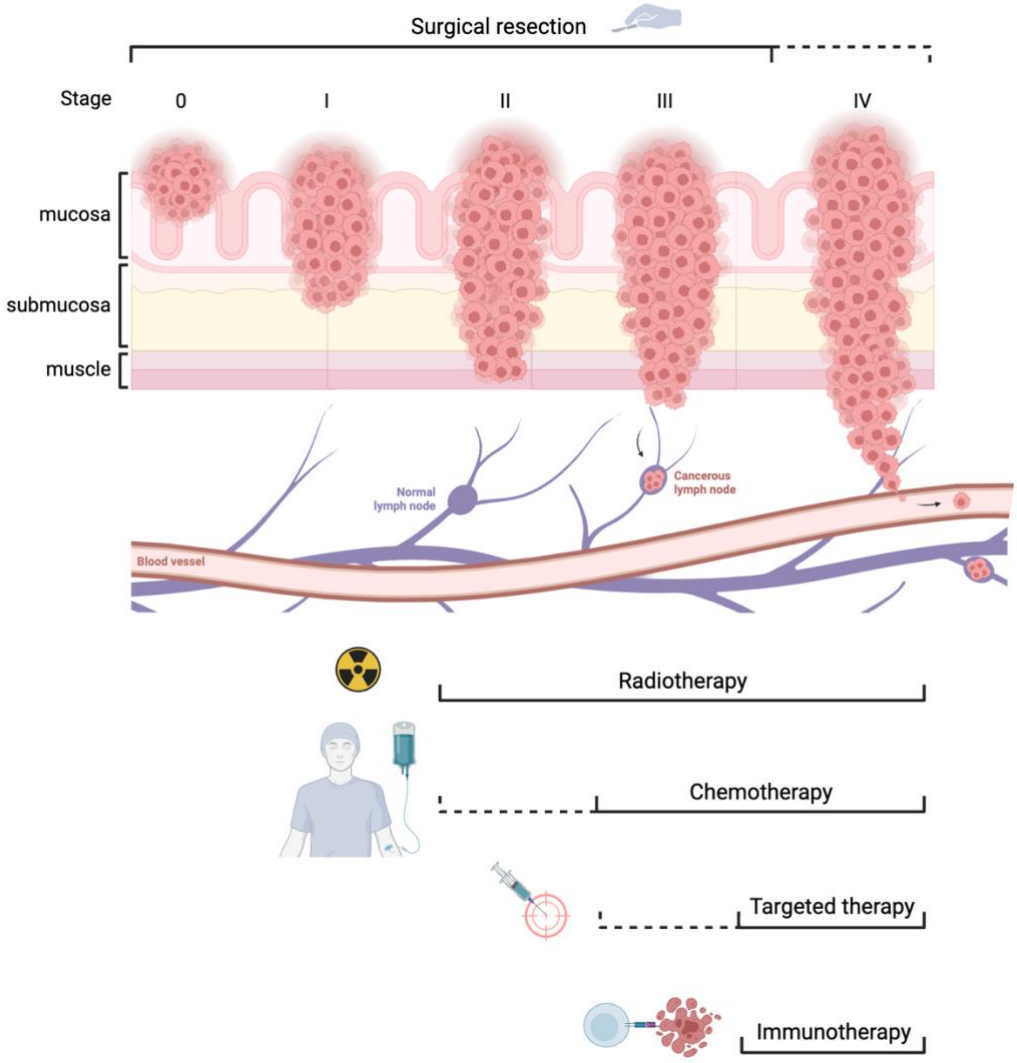

Figure 1 – Colorectal cancer stage-based progression and general treatment recommendations. CRC is classified into stages (0-IV) and the treatment regimen changes according to the progression of the tumor. The main treatment for early stages relies on surgical removal of the tumor, while later stages of CRC often require a combination of different approaches depending on the patient's risk factors as well as the tumor characteristics such as oncogenic mutations, aggressiveness, and location. Created with BioRender.com.

1.2 Hierarchical organization of malignant cells in human colorectal tumors

Colorectal tumors are formed by a heterogeneous cellular population, which is hierarchically organized and governed by a small population of cancer stem cells (CSC) [25]. It is been extensively documented that CSC sub-populations present epigenetic alterations, combined with genetic mutations that, together, result in oncogenic reprogramming fostering cellular plasticity [25-27]. Cellular plasticity is one of the major differences between normal cellular hierarchies and cancer, where cancer cells maintain an intrinsic plasticity that allows them to easily change their phenotype in response to new signals and possibly switch between cellular states [28].

Importantly, this epigenetic reprogramming is closely linked to cancer development and progression [28]. For instance, transcription factors, DNA methylation, and chromatin regulators contribute to malignancy by affecting tumor suppressors and modulating gene expression. Additionally, histone methylation and acetylation play important roles in chromosomal stability, epithelial-mesenchymal transition (EMT), epigenetic silencing, and the promotion of oncogenes. This epigenetic rewriting, necessary for cellular reprogramming, is essential to confer self-renewal and tumor-initiating capacities to transformed cells [26-28].

Cancer stem cells also possess another key characteristic, the ability to adapt to the tumor microenvironment (TME). The TME refers to the intricate network of cells, blood vessels, extracellular matrix, and signaling molecules that surround and interact with cancer cells within a tumor. It can provide signals that maintain the stem-like properties and survival of CSCs. These signals include secreted factors from stromal cells, immune cells, and the extracellular matrix [29, 30]. All these characteristics of CSC have been described as key contributors to tumor aggressiveness, recurrence, and metastasis [27, 31, 32].

CSCs are also involved in therapy resistance. There are two main mechanisms of pharmacological resistance that can contribute to cancer recurrence. One mechanism involves the fact that standard chemotherapy, such as 5-FU and Irinotecan, mainly targets highly proliferative cells and the bulk of the tumor, and CSC can adapt to these treatments by entering into a quiescent state, enabling them to survive drug treatments [32, 33]. The second mechanism involves the plasticity of certain intestinal cell populations that have the ability to de-differentiate themselves, in which differentiated lineages can revert to an immature or progenitor cell fate [27, 34]. Consequently, more differentiated tumor cells can compensate for the loss of CSC and repopulate the tumor with CSCs [27].

The existence of these epigenetically modified and highly tumorigenic cells makes CRC particularly difficult to eradicate. However, given the reversible nature of epigenetic changes, they represent an enormous therapeutic potential. Thus, understanding key epigenetic mechanisms in CCSC and developing new tools to study potential drug targets would provide novel drugs, that in combination with the current treatments, restrict CSC adaptation and therefore, extinguish the root of the cancer.

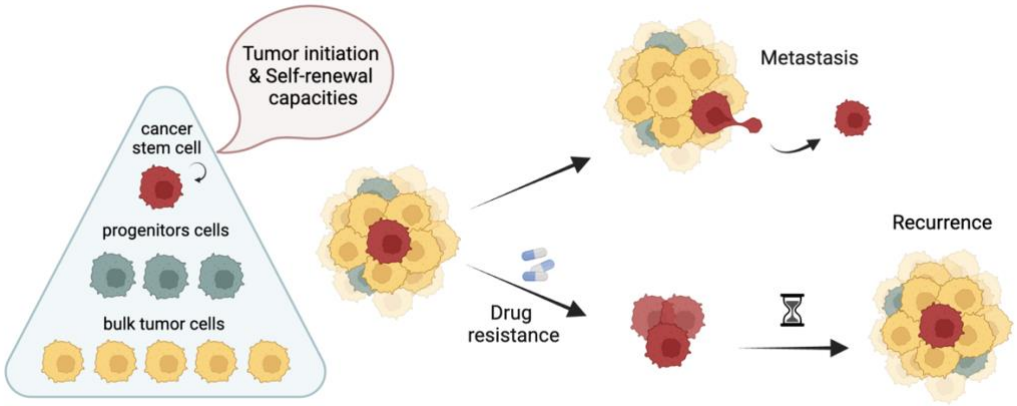

Figure 2 – Hierarchal organization of CRC tumors and CSC capacities. CSC governs the tumor cellular hierarchy, with key features such as self-renewal and tumorigenic properties. This particular cell population has the ability to disseminate at distant organ sites as well as the plasticity to resist chemotherapies and reinstate tumor growth. Created with BioRender.com.

1.3 Epigenetics and colorectal cancer

Epigenetic alterations play a crucial role in cancer initiation and progression due to their involvement in cellular identity and stem cell plasticity [28, 35, 36]. As in multiple types of human cancers, colorectal CSCs (CCSCs) present a unique epigenetic signature that drives malignancy [37]. The epigenetic events characteristic of such a signature control gene expression via mechanisms independent of DNA sequence, including histone post-translational modifications, chromatin loops, histone variant substitutions, and direct DNA methylation on cytosine residues [38, 39].

Of particular interest is DNA methylation, which is generally associated with chromatin compaction, transcriptional repression, and genomic stability. Densely methylated regions, such as CpG islands in promoter regions, are strongly associated with tumor suppressor gene silencing, ultimately promoting malignancy [40-43]. Studies have shown that profound changes in DNA methylation, including mutations down-regulating the DNA methylation machinery, are associated with early events of tumorigenesis, hallmarks of a pre-CSC state in certain cancers, malignant transformation, and reactivation of transposable elements [44-48]. In fact, global genomic hypomethylation is considered a hallmark of CRC initiation [49], and reactivation of Long Interspersed Nuclear Elements (LINEs) retrotransposable elements is one of the phenomena associated with DNA hypomethylation [50]. A high degree of LINE-1 hypomethylation has been shown to be an important feature of early-onset colorectal cancer and is independently associated with shorter survival among colon cancer patients [51, 52].

1.4 LINE-1 retrotransposons and cancer

The human genome contains an extremely large number of repetitive sequences, often described as “junk DNA”, where most of it is derived from transposable elements, estimated to comprise 45% of the human genome [53]. Within the class of transposable elements, we find the retroelements, also called “jumping genes”, which are sequences of DNA widely distributed throughout the whole genome that have the ability to copy themselves within a host genome autonomously through an RNA intermediate, a process called retrotransposition [54]. LINE-1 is the most abundant class of retroelements with an estimated length of 6 kb and occupancy of approximately 17 and 19% of the human and mouse genome, respectively, which makes them the most successful transposable elements in the human genome by mass [53, 55].

LINE-1 contains a 5’-untranslated region (5’UTR), two long open reading frames (ORFs), both of which encode proteins that are required for retrotransposition, and a 3’-UTR followed by a poly-A tail [56, 57]. These elements are normally repressed in homeostasis due to mechanisms such as DNA methylation [45, 58].

When activated, for example by DNA demethylating drugs, LINE-1 sequence is transcribed from the genomic DNA into mRNAs, which are transported to the cytoplasm where the 2 open reading frames go under translation. Two functional proteins are translated, the 41 kDa LINE-1 Open Reading Frame 1 protein (L1ORF1p) and LINE-1 Open Reading Frame 2 protein (L1ORF2), 149 kDa of mass. L1ORF1p is an RNA-binding protein and a nucleic acid chaperone, and L1ORF2p encodes a protein with endonuclease and reverse-transcriptase activities [59-61]. Recently, researchers have discovered the presence of ORF0 on the antisense strand of primate LINE-1 5’UTRs. ORF0 has the ability to generate fusion proteins involving nearby exons and is translated as a short peptide that boosts LINE-1 mobility [62]. Still in the cytoplasm, these two

proteins form ribonucleoprotein particles (RNPs) complexes with the LINE-1 mRNAs that can translocate into the nucleus where the reverse transcription is taking place. LINE-1 DNA sequence can be reintegrated at a new site of the genome through a process termed target-primed reverse transcription (TPRT), whereby reverse transcription of the LINE-1 RNA template is primed from a 3′ hydroxyl at the genomic insertion site [60, 61, 63, 64] (**Figure 3**).

Retrotransposition events mediated by LINE-1 contribute to around 1 out of 250 harmful mutations in humans [65]. These events take place within exons, introns, or regulatory regions of genes, leading to induction or repression on gene expression [66]. The process of LINE-1-mediated retrotransposition not only creates mutations through insertion but also leads to other structural rearrangements in both LINE-1 sequences and the genomic DNA [66-69].

It has been demonstrated that LINE-1 retrotransposition events occur preferentially during the cellular division [70-72]. However, other studies have shown evidence of LINE-1 retrotransposition in non-dividing somatic cells, as well as the association of L1ORF1p with members of the KPNA subfamily, which are nuclear pore proteins [73-75]. Most LINE-1 retrotransposition events in humans occur in somatic cells of the early human embryo [76-80].

Interestingly, a recent study has reported that LINE-1 retrotransposition is more abundant and its promoter is less methylated in healthy colonic epithelium than in other tissues, such as fibroblasts and hematopoietic progenitors [80]. The authors suggest an incomplete re-methylation process that would occur following early embryonic stages at the promoter of retrotransposition-competent LINE-1 within the colonic epithelium lineage [80]. This insufficient LINE-1 re-methylation pattern was not observed in other tissues, underscoring its colon-specific nature and the significance of investigating this phenomenon in CRC.

Despite the abundance of LINE-1 copies within our genome, not all LINE-1 copies are competent for retrotransposition. Indeed, as a result of TPRT and decay over time, most LINE-1 copies are inactivated by truncations, internal rearrangements, and mutations [53, 81]. Of the more than 500,000 LINE-1 elements in the human genome, less than 100 copies are functional, called "hot LINE-1" sequences [82, 83].

LINE-1 retrotransposition takes place across different types of cancers [80, 84-87]. Research indicates that somatic LINE-1 insertions predominantly occur in epithelial cancers, like those in the gastrointestinal tract. The number of LINE-1 insertions varies within epithelial tumors, with some having more than 50 somatic insertions and others having none. Moreover, specific clonal somatic insertions identified in esophageal and gastric tumors appear at low frequencies in normal tissue. This suggests that a normal cell harboring a somatic LINE-1 insertion might experience clonal expansion within the context of cancer [88-90]. The existing literature still diverges on whether LINE-1 insertions represent "driver" or "passenger" mutations in cancers. On one hand, most somatic LINE-1 insertions found in epithelial cancers are considered as passenger mutations [91]. However, certain somatic LINE-1 insertions, such as those reported to inactivate the tumor-suppressor genes APC and PTEN, suggest that they potentially drive tumorigenesis [92-94]. Additionally, L1 retrotransposition events have been systematically explored in cancer tissues, showing a higher burden of L1 retrotransposition, which often leads to the alteration of cancer genes [95].

Specifically in CRC, emerging data gathered through a multi-omics approach on clonal organoid cultures established from human colonic adenoma, carcinoma, and healthy crypts, show that the rate of LINE-1 retrotransposition in primary CRC samples is tenfold higher than in normal colonic tissues from the same patient [80]. Interestingly, their results suggest that CRC appears as

an accommodating context for LINE-1 events. Curiously, 97% of these LINE-1 retrotransposition events detected in primary CRC samples were identified as clonal events shared across all tumors, suggesting that such clonal retrotransposition events occur early in the CRC tumorigenesis cascade due to the epigenetic reprogramming characterizing tumor initiation [80, 95, 96].

Furthermore, an association has been established between elevated levels of LINE-1 mRNA, increased expression of L1ORF1/2 proteins, and various cellular processes such as apoptosis, DNA damage and repair, cellular plasticity, and stress responses. This increased expression has also been implicated in tumor progression [97-100]. DNA damage resulting from either genome-wide or interspersed repetitive sequence hypomethylation has the potential to trigger an inflammatory microenvironment, often referred to as viral mimicry, which will be discussed later [101, 102].

Importantly, previous literature has established a correlation between enhanced LINE-1 retrotransposition and L1ORF1p overexpression with CCSC development [45, 46, 103]. Yet, most of the pathways leading to LINE-1 activation in cancer remain unknown.

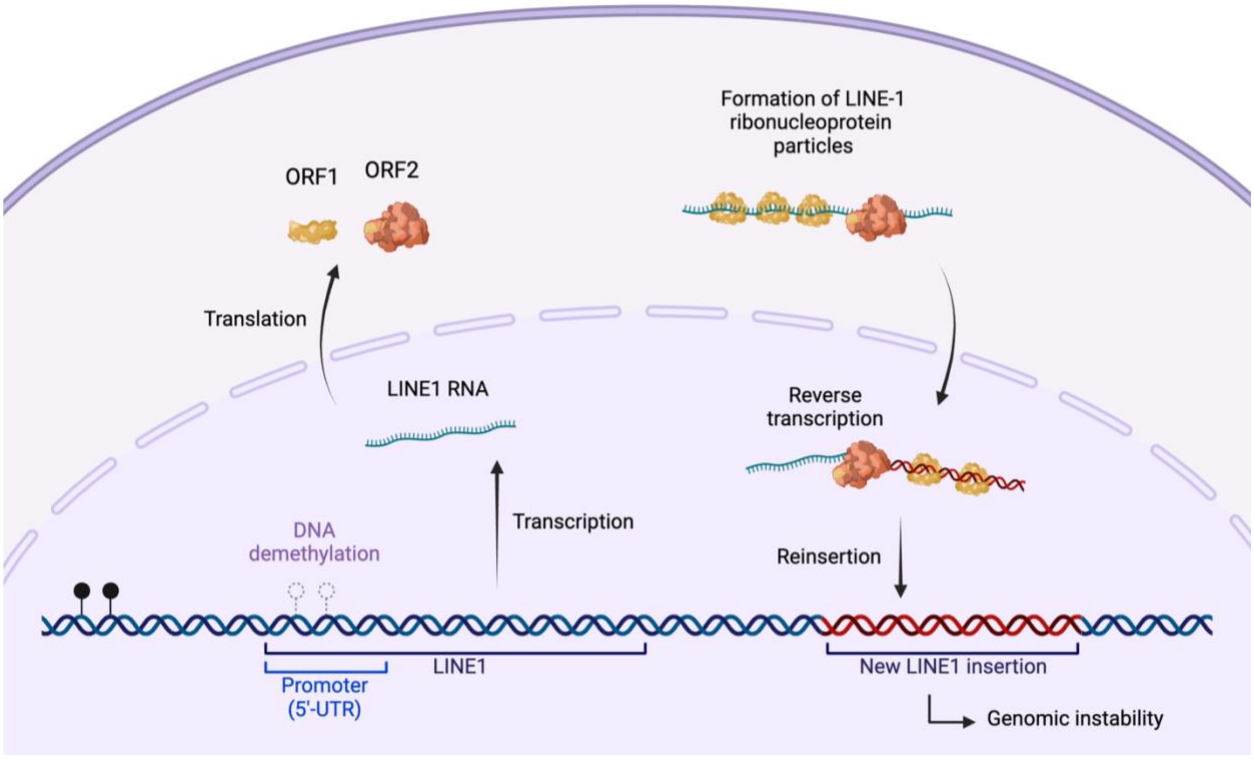

Figure 3 – LINE1 retrotransposition cycle. As previously described, LINE-1 are autonomous elements, possessing the ability to self-propagate independently of other transposable elements. Following demethylation, LINE-1 elements transcription is reactivated, and open reading frames are translated into L1ORF1p and L1ORF2p in the cytoplasm. Both proteins are critical for the formation of a LINE-1-RNP intermediate complex, which is imported into the nucleus where the reverse transcription occurs and the new copy of LINE-1 DNA is reinserted into a new genomic location. Created with BioRender.com.

1.5 L1ORF1 represents a key therapeutic target for colorectal cancer

Considering the increased mobilization of LINE-1 upon global DNA demethylation, and the role of such retroelements in the initiation and progression of multiple human cancers, including CRC, LINE-1 machinery poses an appealing pharmacological target for inhibiting the onset and evolution of CRC.

Notably, recent studies have suggested that L1ORF1p RNA-binding capacity can be inhibited by small molecules via RMM-CTD domains [104]. Considering the chaperone activity of L1ORF1p, it is expected that such small molecule ligands would present structural similarities with RNA (*i.e.* nucleoside analogs).

However, targeting L1ORF1p is not expected to be used as a monotherapy, but in synergy with common genotoxic drugs (Oxaliplatin, 5-FU, Irinotecan), or hypomethylating agents (5-Azacytidine) already approved in the clinic [105, 106]. Interestingly, hypomethylating agents acting through DNA methyltransferases (DNMTs) inhibition have already been shown to increase retrotransposons mobility in cancer patients, potentially contributing to CSC biogenesis and clonal diversification within tumors over the course of treatments. Ultimately, the use of novel L1ORF1p disruptors would improve the efficacy of standard treatments for CRC.

1.6 LINE-1 activation and viral mimicry

The conceptualization of viral mimicry is relatively recent and can be summarized as being a cellular antiviral immune response triggered by endogenous stimuli, typically induced by cytosolic nucleic acids derived from aberrantly transcribed endogenous retrotransposons. During a retrotransposition event, retroelements produce double-stranded RNAs (dsRNAs), RNA:DNA hybrids, and L1 cDNA fragments that can be detected by innate immune receptors, which

otherwise would detect nucleic acids from pathogens such as viruses. This activation of immune pathways often leads to death of cells due to the activation of cytokines and IFN response [96, 107].

Interestingly, emerging data have also revealed favorable outcomes of increasing dsRNA levels from human endogenous retrovirus (hERV), LINEs, and SINEs after treating cancer cells with DNMTs inhibitors [107, 108]. For example, 5AZA treatments of patient-derived CRC samples induce the demethylation and expression of endogenous retroelements causing cytosolic accumulation of dsRNA species. These are sensed as viral infection by innate immunity pathways, leading to the production of IFNβ, initiation of an Interferon-Stimulated Genes (ISG) response, and immunogenic cell death in cancer cells, including CSC populations [109, 110]. In human-to-mouse xenograft models, this phenomenon increased the recruitment and the activation of Natural Killer cells and CD8+ T cells within tumors. This immune reaction was associated with a decrease in the size of tumor xenografts and an extension of mouse survival [111, 112]. Specifically, in colorectal cancer, stimulation of endogenous elements, due to DNA hypomethylation, has been shown to sensitize cells to checkpoint inhibitors, such as CTLA-4 and PD-1 [110, 113].

Endogenous retroelements have recently been proposed as intracellular “alarms” to trigger innate immune response when homeostasis is disrupted in the cell, such as in a tumorigenic process [114]. The presence of immunogenic endogenous retroelements influences the inflammation by amplifying the IFN response, where they function as enhancers of the ISGs gene expression [115]. The “fire alarm hypothesis” suggests that endogenous elements serve as alarms due to three main characteristics. First, they are globally distributed throughout the genome. Second, they are capable of activating an innate immune response. Lastly, they evolved to be maintained silent within the human genome by a broad range of reversible molecular mechanisms [114]. This

hypothesis emphasizes that the defensive mechanisms evolved to combat viral infections are also harnessed by the cells to detect and suppress the early stages of cancer development (**Figure 4**).

Interestingly, independent studies showed that reverse transcriptase (RT) inhibitors downregulate viral mimicry by decreasing cytoplasmic double-stranded nucleic acid species generated by LINE1 ORF2 RT activity [116, 117]. Despite the reported benefits from transposable elements RNA expression, with viral mimicry stimulating antitumor immune response [109], different groups are currently developing small molecules blocking reverse transcriptase encoded by retrotransposable elements based on classical nucleoside [118] or non-nucleoside structures [119]. While such inhibitors may help to decrease high rates of LINE-1 retrotransposition in CRC, they could also downplay innate immune recognition and elimination of early neoplastic lesions, the "fire alarm" triggered by endogenous retroelements [114]. In this regard, Hepatitis B patients from a large cohort study (>35,000 individuals) undergoing long-term RT inhibitor treatments showed increased CRC incidence compared to untreated subjects [120].

Therefore, identifying new small molecules that can specifically target L1ORF1p to curb LINE-1 reintegration and genomic plasticity, while promoting their epigenetic de-repression and associated viral mimicry, could represent an attractive approach to block CSC plasticity and biogenesis, and ultimately reduce the risk of acquisition of therapeutic resistance and tumor relapses.

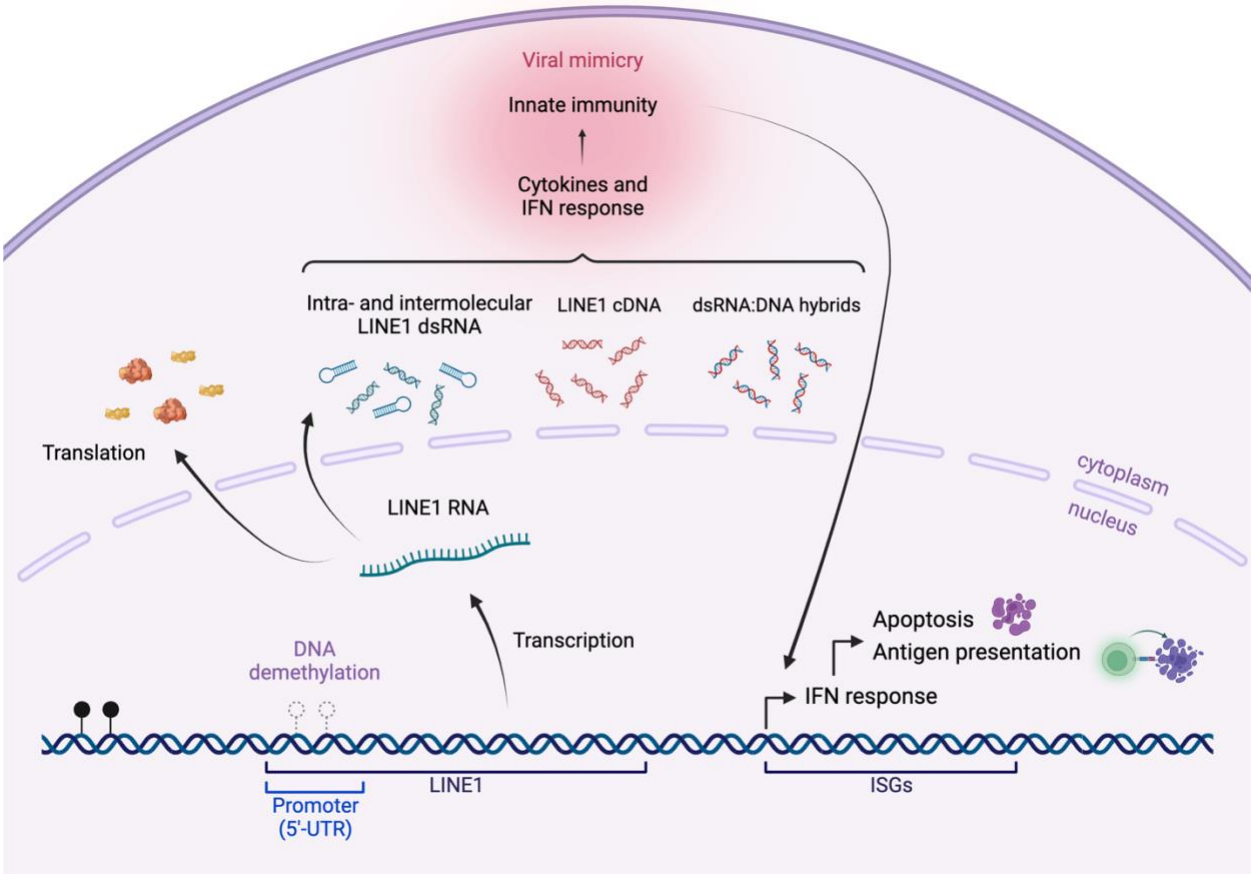

Figure 4 – Viral mimicry induced by the activation of LINE-1 retrotransposons. Following demethylation, LINE-1 transcription is driven by a promoter located in their 5'UTR region (5'UTR). Upon modifications stabilizing the LINE1 transcripts, LINE1 open reading frames are translated in the cytoplasm. LINE1-derived double-stranded RNA (dsRNA) generated by inter or intramolecular complementarity, cDNA, and LINE1 RNA:DNA hybrids in the cytoplasm can trigger an antiviral-like innate immune response, activating an interferon response, which will lead to apoptosis and antigen presentation, both resulting in cell death. Created with BioRender.com.

Hypothesis and Objectives

2.1 Hypothesis

I hypothesize that targeting LINE-1 activity in CRC could contribute to a better understanding of the impact of retroelements in cancer. It will also help define whether endogenous retroelements, such as LINE-1 retrotransposons, must be considered as good or bad in the development of new therapeutic approaches against CRC.

2.2 Objectives

To contribute to advancing technical aspects of LINE-1 and retroelement-based drug discovery research in CRC, as outlined by the following objectives:

Objective 1: Characterization of a new clinically safe drug that activates transposable elements' expression in colon cancer.

Objective 2: To develop new tools to downregulate retroelement mobility in colon cancer.

Objective 3: Establishment of colonic organoids derived from healthy tissues as a normal counterpart tool to study the toxicity of new drug candidates, including retroelement-modulating compounds.

Materials and Methods

3.1 Cell culture

HIEC cell culture

The normal intestinal epithelium cell line, HIEC, was cultured in Opti-MEM Reduced Serum with 1% HEPES and 1% L-glutamine mixed with 5% Wisent Premium and 10 ng/mL Epithelial Growth Factor. The cells were cultured in 10 cm culture plates at 37ºC 5% CO_2. The media were changed every 3 days. The cells were passed every 5 days at a 1:3 ratio.

HCT116 cell culture

The human colorectal adenoma cancer cell line, HCT116 (male), was cultured in McCoy's 5A Medium with L-Glutamine mixed with 10% Fetal Bovine Serum. The cells were cultured in 10 cm culture plates at 37ºC 5% CO_2. The cells were passed every 5 days in 1:10 ratio and the media were changed 3 days after passage.

HT29 cell culture

The human colorectal adenoma cancer cell line, HT29 (female), was cultured in McCoy's 5A Medium with L-Glutamine mixed with 10% Fetal Bovine Serum. The cells were cultured in 10 cm culture plates at 37ºC 5% CO_2. The cells were passed every 5 days in a 1:10 ratio and the media were changed 3 days after passage.

HeLa cell culture

The human cervical adenoma cancer cell line, HeLa (female), was cultured in DMEM Medium with 10% Fetal Bovine Serum. The cells were cultured in 10 cm culture plates at 37°C 5% CO_2. The cells were passed every 4 days in a 1:10 ratio and the media were changed 2 days after passage.

t-hESC cell culture

The transformed human pluripotent stem cells (t-hESCs) were cultured in mTSER medium with mTSER supplement in a 6 well-plate coated with Matrigel at 37°C 5% CO_2. The medium was changed the day after the cells were passed. The cells were passed in a 1:5 ratio every 5 days using 1X Collagenase IV in clumps through scraping off the cell surface.

293FT cell culture

The 293FT cell line is a fast-growing, highly transfectable clonal isolate derived from human embryonal kidney cells. The 293FT cells were cultured in DMEM medium mixed with 10% Fetal Bovine Serum. The cells were cultured in 10 cm culture plates at 37°C 5% CO_2. The cells were passed every 5 days in a 1:10 ratio and the media were changed 3 days after passage.

MC38 and CT26 cells culture

Mouse colorectal adenocarcinoma MC38 (C57BL/6) and CT26 (BALB/c) cells were cultured in DMEM and RPMI media supplemented with 10% Fetal Bovine Serum, 2 mM Glutamine, 0.1 mM Nonessential Amino Acids, 1 mM Sodium Pyruvate, and 10 mM HEPES at 37°C 5% CO_2. The cells were passed every 5 days in a 1:10 ratio and the media were changed 3 days after passage.

3.2 Patient-derived colon samples culture

Briefly, patient-derived colon samples were divided into 3 pieces. One section was snap-frozen for RNA or protein extraction. The second section was fixed in 10% formalin for 24 hours and then transferred to 70% ethanol for subsequent steps in the immunohistochemistry process. Lastly, the third section was mechanically dissociated into smaller fragments, followed by enzymatic digestion. Subsequently, isolated crypts were embedded in Matrigel and seeded in 24-well plates. The organoids were cultured at 37^{o}C 5% CO_2, split every 4-6 days, and the media changed three times a week. More details of each step can be found in "Results 4.3" section of this thesis.

3.3 *In vitro* drug-dose response treatment

The drug-dose response was performed by seeding 8,000 cells of HIEC and 5,000 cells of HCT116, HT29, and HeLa per well in their respective 96-well plates. After 24 hours of seeding, the cells were treated with 1% DMSO (control) along with drug dose between 1 μM to 10 μM of Dihydroergotamine and Ubrogepant. The cells were treated for 48 hours at 37^{o}C 5% CO_2. After 48 hours of drug treatment, the cells were washed with 1X PBS and fixed with 3% paraformaldehyde for 10 minutes at room temperature.

3.4 *In vitro* drug treatments

The drug treatments were performed by adding sterile cover slips in each well of a 6-well plate and seeding 800,000 cells of HIEC and 500,00 cells of HCT116 and t-hESC per well in their respective plates. After 24 hours of seeding, the cells were treated with drug for 48 or 72 hours at 37^{o}C 5% CO_2. After the drug treatment was done, the cells were washed with 1X PBS and fixed with 3% paraformaldehyde for 10 minutes at room temperature.

3.5 Western blot

Total protein samples were prepared in 4X Laemmli Buffer (0.1% β-Mercaptoethanol, 10% Glycerol, 0.005% Bromophenol Blue, 62.5mM Tris-HCl pH 6.8, and 1% SDS) and sonicated (30% amplitude 5 second pulses and 3 second rest). Prior to running the Western blot, the total protein samples were denatured in 95ºC for 5 min. The Amersham ECL Rainbow Marker Ladder – Full Range (Millipore Sigma) and samples were run in 12.5 % polyacrylamide gels. After protein migration and transfer, the nonspecific proteins were blocked with 5% skimmed milk or 5% Bovine Serum Albumin (BSA) in 1X PBS 0.1% Tween-20 for 1 hour followed by primary antibody incubation, diluted in blocking buffer in 4ºC overnight, followed by an additional primary antibody incubation for 1 hour at room temperature. After the primary antibody incubation, the membranes were washed with 1X PBS 0.1% Tween-20 for 3 sequential washes. The membranes were incubated in horseradish peroxidase-conjugated secondary antibodies which was diluted in 1X PBS 0.1% Tween for 1 hour at room temperature. This was followed by 3 consecutive washes with 1X PBS 0.1% Tween. Visualization of the membranes were done by addition of Immobilon® Forte Western HRP Substrate. Images were taken using ChemiDoc MP Imaging System (Bio-Rad). The blots were quantified using Image J software (National Institutes of Health).

3.6 Docking analysis of small molecule ligands and L1ORF1 RNA binding domains

A total of 9,181 compounds from the Drugbank virtual library were docked into the RMM-CTD domains of L1ORF1p (PDB #2LDY), which is the active site region known for interaction with small molecules [121]. The generated SMILES of drug compounds were downloaded directly from the Drugbank website. RMM-CTD and ligands were prepared into PDBQT files using PyRX ensuring that proteins contained each atom's respective hydrogens and water molecules were

discarded [122]. Subsequently, protein-ligand docking was performed by assigning each compound with an X-score using Autodock Vina. Autodock Vina scoring considered the gaussian steric interaction, finite repulsion, piecewise linear hydrophobic, entropic term and hydrogen bond interaction between the protein and the ligand [123, 124] with an assumption of the receptor as a rigid protein while compounds are flexible molecules with a range of 0 to 32 active rotatable bonds [124, 125]. Once the proteins and ligands were both ready for docking, using PyRx, Autodock Vina was run. Each run used an exhaustiveness of 50 in triplicates. Each compound docked to the receptor were given a score (ΔG) based on the intermolecular and intramolecular total contribution and ranked [124]. The predictive binding energy was calculated using the following equation: $Keq = 10{-}\Delta G/1.36$. Validation of protein-ligand interactions and visualization of main residues putatively involved were performed using LigPlot and Chimera [126].

3.7 Pan assay interference compounds (PAINS)

The hit compounds obtained from the virtual docking, described in Section 3.5 Docking analysis of small molecule ligands and L1ORF1p RNA binding domains, were filtered using the PAINS to identify compounds that appear as frequent hitters, also called “promiscuous compounds”. These compounds are commonly shown as hits in many biochemical high throughput screenings as they have been reported as highly reactive compounds. Therefore, the PAINS filter was used to remove potential false positive hits from the virtual drug screening (PAINS website: https://www.cbligand.org/PAINS/login.php). The list of hit compounds with their respective smiles’ formulas was uploaded to the PAINS remover website and then the list of structures of compounds that were filtered out by the filter was provided.

3.8 Indirect immunofluorescence

Experimental samples were prepared in 6-well plates, as described in the section 3.2 *In vitro* Drug Treatments. Immunofluorescence was performed to observe ORF1 expression and sub-cellular localization in HCT116 and t-hESC cells. As the initial steps for immunofluorescence staining, cells were washed with 1X Perm wash followed by primary antibody incubation overnight at 4ºC. After primary antibody incubation, cells were washed with 1X Perm wash and incubated with their respective secondary antibody, Alexa Fluor 647 listed in Table 2, at room temperature for 1 hour. Nuclei staining was done using Hoechst for 10 minutes at room temperature or using Prolong Diamond Antifade Mounting media with DAPI.

3.9 Subcellular protein localization analysis

Cells were obtained after drug treatment was done, following the steps described in Section 3.3 *In vitro* drug treatments, and stained following steps described in Section 3.6 Immunofluorescence. Images were taken using Zeiss AxioImager M2 at the Cell Microscopy core of the University of Ottawa. Image files were analyzed using CellProfiler. L1ORF1p was quantified in both the nucleus and cytoplasm for each drug treatment. DMSO treated cells were used as a control.

3.10 Plasmid amplification and purification

L1ORF1 shRNA oligos were inserted into lentiviral vector (Addgene: 10878) following the Addgene protocol (pLKO.1 – TRC cloning vector, protocol version 1.0, December 2006). Competent bacteria were transformed with these lentiviral constructs, and inoculated overnight in LB broth with 100 µg/mL of ampicillin at 37ºC with continuous shaking. After inoculation, the plasmid was extracted and purified from the bacterial samples using QIAprep Spin Miniprep kit.

To verify the purity of lentiviral plasmids, they should be digested with specific restriction enzymes and run in 1% agarose gel for 1 hour. Only bands corresponding to the predicted sizes of the digested plasmid are expected.

3.11 LINE1 reporter transfection

HCT116 cells were seeded 24 hours before the transfection onto 10 cm dish at 60 to 70% confluency. Transfection medium were prepared using 53 µL of Lipofectamine LTX reagent, 18 µL of Plus reagent mixed with 12 µg of LINE-1 reporter vector in OptiMEM Free medium and incubated for 10 minutes at room temperature. In a drop-wise manner, transfection medium was added to the 10 cm dish containing HCT116 cells and incubated overnight at 37ºC 5%CO_2. The next day medium was changed, and cells were subjected to 1 µg/mL of puromycin selection for 7 days. Plates were checked for GFP positive cells on ImageXpress PICO.

3.12 High content imaging and analysis

Visualization of cell counts, immunofluorescence and organoid counts were performed using Cellomics Array Scan VTI (Thermo Fisher) from Stem Core Laboratory at The General Ottawa Hospital. Analysis and quantifications were done using HCS Studio™ Software.

3.13 RT-qPCR analysis

Total RNA was extracted and purified using RNeasy Mini Kit (Qiagen) by following the manufacturer's protocol. Quantification of purified RNA was performed using a Nanodrop 2000 Spectrophotometer (Thermo Scientific). cDNA synthesis was done using 500 ng of purified RNA and Superscript III FirstStrand Synthesis (Life Technologies) followed by running samples in

Thermocycler (Thermo Fisher). The synthesized cDNA was mixed with PowerSybr Green PCR master mix (Life Science) and its corresponding primers seen in Table 1. The RT-qPCR were run in ABI 7500 Real-Time PCR system (Applied Biosystems). All data were normalized to GAPDH, and fold changes were calculated based on the method described by Pfaffl in Nucleic Acids Res (Pfaffl, 2001).

3.14 Transcriptome profiling and bioinformatics analysis

Next-generation RNA sequencing was performed at the StemCore facility of the Ottawa Hospital Research Institute (OHRI) on an Illumina NextSeq 500 platform according to 1 x 75bp cycles of single-end sequencing, yielding 25 million reads per sample. PhiX ssDNA was spiked in each sample and used as a technical control for clustering reactions. Upon alignment of sequencing data, control vs. treated, transcriptomes for each cell line were compared and significantly modulated genes ($p<0.05$) were identified using the Salmon transcript abundance method [127]. RNA-seq alignment and specialized bioinformatics analyses were performed with the support of the Ottawa Bioinformatics Core Facility. Transposable element transcript profiling was conducted using the TEtranscripts package, as previously described [128]. Volcano plots were generated with the Enhanced Volcano package with points colored relative to p-value and $\log_2$FoldChange cutoffs. Gene set enrichment analysis (GSEA) was performed on differentially expressed genes from VXN versus DMSO treatment in HT29, HCT116, and t-hESC cell lines using GSEA Software version 4.0.3 [129].

3.15 Immunohistochemistry

Human primary colon carcinoma and mouse syngeneic primary CRC tumours were clean flushed with 1X PBS followed by 10% buffered formalin fixation for 24 hours at 4°C. Fixation stopped with 70% ethanol and the samples were sent to Louise Pelletier Histology Core Facility at the University of Ottawa for sectioning, paraffinization, de-paraffinization, and antigen retrieval. The tissue samples were sectioned at 4 microns and embedded on microscope tissue slides. Each tissue samples were quenched with 0.1 M glycine solution for 30 minutes at room temperature. The slides were blocked with 2% BSA at room temperature for 30 minutes. Information on all primary antibodies used and working dilutions is available in Table 2. The slides were incubated overnight at 4°C followed by consecutive washes on 1X PBS. The slides were incubated with their respective secondary antibodies (anti-rabbit Alexa Fluor 488 and 647, anti-mouse Alexa Fluor 488 and 647) at 1:500 in a 1% BSA solution for 1 hour at room temperature. At the end of the 1-hour incubation, the slides were washed three consecutive times for 15 minutes with 1X PBS. The preservation of fluorescence and prevention of photobleaching was done by the addition of Vectashield Antifade Mounting Medium with DAPI or Prolong Diamond Antifade Mounting Medium with DAPI. Images were taken with an ImageXpress Pico High-Content imaging system (Molecular Devices), acquired, and analyzed using CellReporterXpress software.

3.16 *In vivo* CRC tumor engraftment assays

All *in vivo* procedures and protocols were approved by the University of Ottawa Animal Care Committee. Untreated cancer cells were dissociated and resuspended in a 1:1 HBSS:Matrigel mixture prior to subcutaneous injection into the flanks of primary C57BL/6 and BALB/c mouse recipients, respectively (6 to 8-week-old females), at a density of $1x10^6$ cells per site. Seven days

post-injection, daily doses of vanoxerine (25 mg/kg) or control saline (HBSS vehicle) were intraperitoneally injected into tumor-bearing animals for 10 days. Primary tumour growth was measured daily following palpable tumour detection using a digital caliper. The ellipsoidal tumour volume was calculated according to Volume = (Length x Width x Width)/2. Mice were scrutinized for potential changes in behavioral and clinical indicators, including weight loss, fecal consistency, rectal bleeding, movement disorder, facial grimace, abnormal respiration, hunching, piloerection, agitation/aggressivity, food consumption and grooming habits during and after drug administration. At endpoint, the mice were sacrificed, and tumours were harvested. Tumours were washed briefly in cold 1x PBS and fixed overnight immersed in 10% neutral buffered formalin in the dark at 4^{o}C. The following day, all tissues were transferred to 70% ethanol and stored in the dark at 4^{o}C until further processing.

3.17 Statistical analysis

The statistical analysis was all performed using GraphPad Prism 8 software unless otherwise mentioned (GSEA). One-way ANOVA was used to compare the different experimental groups to control in drug treatment *in vitro* and immunofluorescence. Unpaired t-test were used for RT-qPCR analysis. Data are all represented as mean ±SEM and p-values lower than 0.05 are considered significant. “n” denotes the number of independent biological replicates.

Results

4.1 Objective 1: Characterization of a new clinically safe drug that activates transposable elements' expression in colorectal cancer

DNA methyltransferase inhibitors (DNMTis) were previously shown to restore the expression of tumor suppressor genes silenced by promoter methylation in cancer [130]. Previously in our lab, we demonstrated that inhibiting G9a, a histone methyltransferase responsible for H3K9 mono and di-methylation, not only markedly decreased tumor-initiating activity of patient-derived CRC stem cells, but also significantly reduced DNA methylation in L1ORF2 and 5'UTR regions of LINE-1 elements. This resulted in notable increases in hERVs and LINE-1 transcripts, indicating the reactivation of retrotransposable elements due to DNA hypomethylation [131].

Subsequently, through a phenotypic drug screening assay, we discovered Vanoxerine (VXN) as a new clinically safe compound that decreases G9a levels and alters CCSC functions. This compound was shown to decrease H3K9me2 deposition in t-hESC (a transformed variant of human embryonic stem cells) and HT29 (a human colon cancer cell line) (**Figure 5A and 5B**). T-hESC has been previously documented as a surrogate model of CSCs in culture and predictive of drug response in the context of neoplastic stemness [132-135]. 5-Methylcytosine DNA methylation (5-meC) is decreased by VXN treatment, similarly as what is seen with BIX-01294, a G9a direct inhibitor (**Figure 5C**).

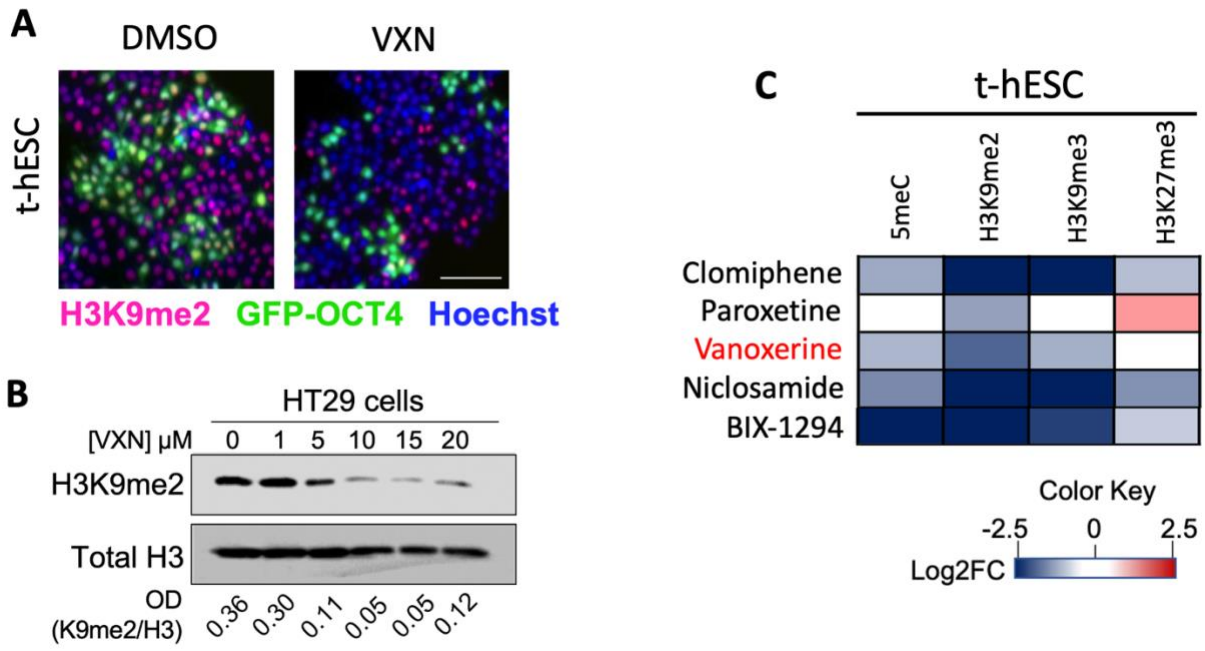

Figure 5 – The effects of VXN on H3K9me2 deposition and 5-cytosine DNA methylation levels in cancer models. A) Micrographs showing inhibitory effect of VXN (5 µM, 48h) on OCT4 expression (pluripotency) and H3K9me2 deposition in t-hESCs (scale bar: 100 µM). B) Dose-response inhibition of H3K9me2 levels in HT29 (CRC cells) upon VXN treatment (48h). Average optical density ratios for H3K9me2 vs. loading control total H3 is presented (n=3). C) Heatmap of the mean immunodetection signal from validation experiments assessing total 5-meC and histone marks H3K9me2, H3K9me3, and H3K27me3 levels in t-hESC treated with VXN, 2 other hit compounds from the phenotypic drug screening assay (Clomiphene and Niclosamide), and Paroxetine (random drug) (5 µM, 48h) vs. DMSO control (n=3, L2FC of OD ratios drug/DMSO, cut off: >0.25). BIX-02492 (1 µM, 48h) was used as a positive control.

Aiming to identify the differential expression of Transposable Elements (TE) across cell lines, RNA-sequencing was performed to compare different cell lines treated with drugs compared to DMSO control. VXN treatment increased TE in HT29 and HCT116. The same increased was observed when t-hESC were treated with VXN and BIX-01294 (**Figure 6**). We observed that VXN globally increased TE expression in HT29, HCT116 and t-hESC cells, akin to the effect of BIX-01294.

Previous studies have reported an immune signaling upregulation triggered by DNMTis in cancer cells [109, 110]. To further study the effects of VXN in HT29 cells, specifically the impact on genes related to immune response, more precisely the type-1 interferon (IFN-1) response, GSEA analysis was done to study gene signatures characteristics of IFN-1 response. Gene sets related to IFN-1 and viral defense responses were highly enriched within the VXN-induced transcriptional signature (**Figure 7A**). The colorectal cancer cell line (HT29) exhibited a significant upregulation on INF-1 genes upon drug treatment, which was not seen in the normal intestinal cell line (HIEC). That difference in the drug effect indicates a cancer-selective influence of VXN.

Consistent with the role of L1ORF2p on viral mimicry induction, blocking retroelement transcription by co-treating these cells with reverse transcriptase inhibitors (RTi: Zidovudine and Nevirapine) suppressed VXN-dependent induction of IFN-1 response markers in HT29 cells (**Figure 7B**). These two reverse transcriptase inhibitors act through two different mechanisms. Zidovudine, a Nucleoside Reverse Transcriptase Inhibitor (NRTI), competitively inhibits the enzyme and acts as a chain terminator of DNA synthesis. Nevirapine, a Non-nucleoside Reverse Transcriptase Inhibitor (NNRTI), functions as a non-competitive substrate analog, binding directly to the enzyme's catalytic site, blocking its activity.

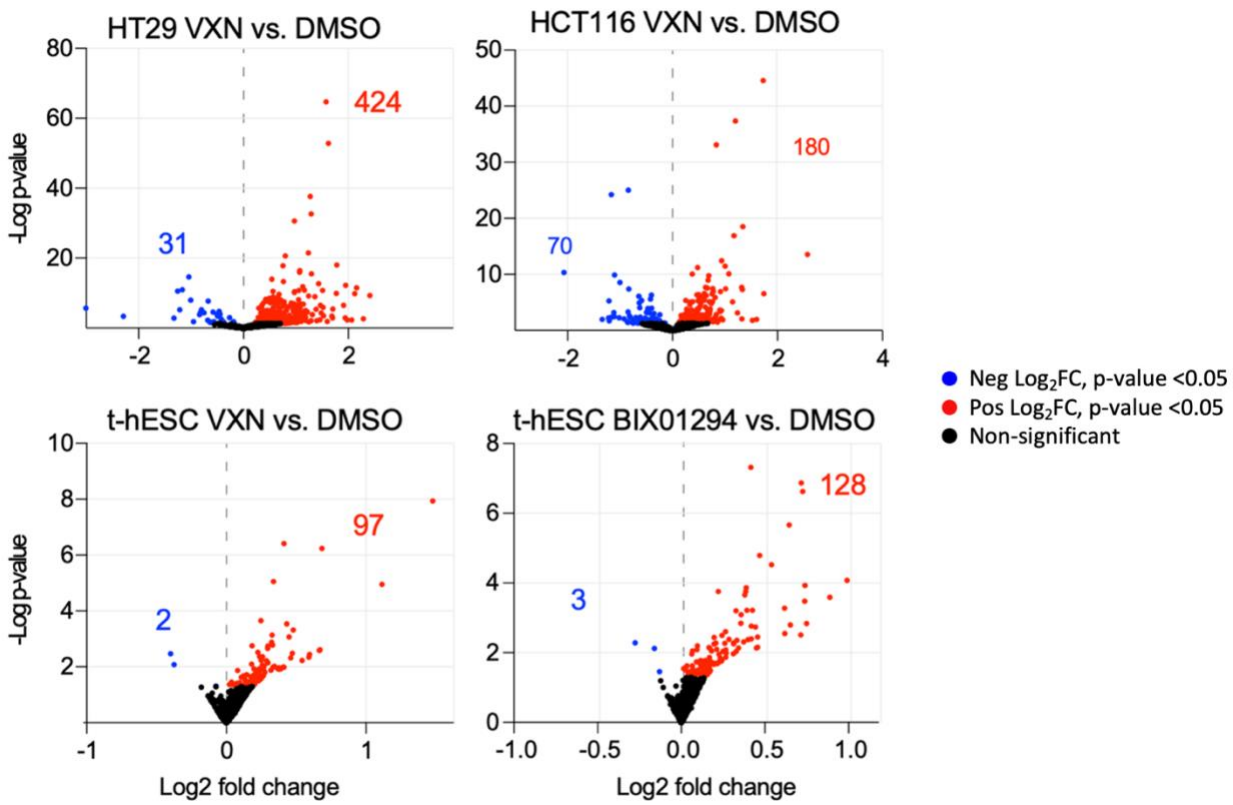

Figure 6 – Investigating the effect of BIX and VXN on TE activity in HT29, HCT116, and t-hESC cells. Differential expression of TEs in VXN-treated (10 μM, 48 h) HT29 and HCT116 cells, as well as in t-hESC treated with VXN (10 μM, 48 h) or BIX-01294 (1 μM, 48 h) vs. respective DMSO controls (n ≥2, p<0.05).

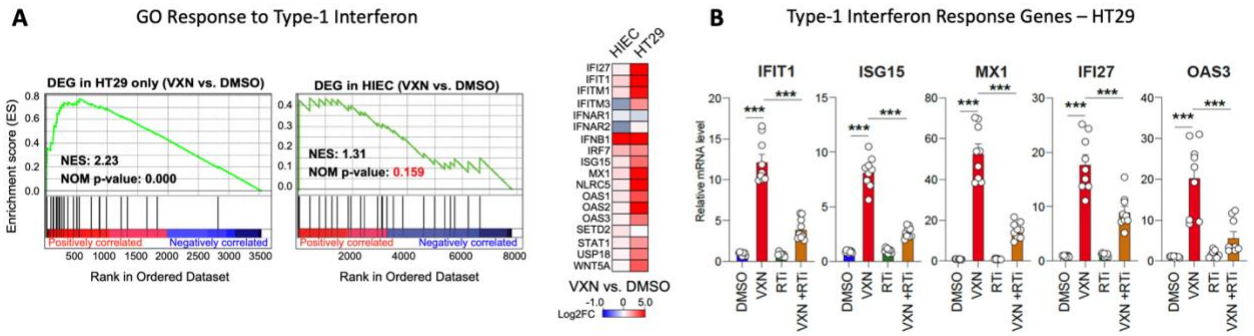

Figure 7 – **Type-1 interferon response in HT29 treated with VXN. A)** GSEA plots showing a positive correlation between genes selectively modulated by VXN in HT29 cells (vs. DMSO, $p<0.05$) and gene signatures characteristic of type-1 interferon response. Such a profile is not observed at a significant level in VXN-treated HIEC cells (vs. DMSO) (NOM p=0.159). The expression of all type-1 interferon response genes highlighted by GSEA is presented in a heat map (L2FC of FPKM values) following VXN treatments (vs. DMSO) in HIEC and HT29 cells. **B)** qPCR analysis of type-1 interferon response genes in HT29. Analysis of IFIT1, ISG15, MX1, IFI27, and OAS3 genes expression in HT29 cells treated with VXN (10µM) and/or reverse transcriptase inhibitors (RTi: Zidovudine and Nevirapine: 20µM) vs. DMSO (48h, n=9, ***: $p<0.0001$).

This immune response upregulation was also confirmed by *in vivo* experiments. Briefly, colorectal adenocarcinoma MC38 (C57BL/6) and CT26 (BALB/c) cells mixed with Matrigel and injected subcutaneously into the flanks of C57BL/6 and BALB/c mouse recipients, respectively. Seven days post-injection, daily doses of VXN (25mg/kg) or control saline were intraperitoneally injected into tumor-bearing animals for 10 days. On day 18, tumors were surgically extracted and analyzed. High-content imaging analysis of CRC tumor sections showed a significant increase in CD8-positive cells in both MC38 and CT26 tumors (**Figure 8A**). Certified histopathological analysis of CRC tumor sections supported the enhanced presence of tumor infiltrating lymphocytes in VXN-treated animals compared to vehicle controls (**Figure 8B**). Expression analysis of a panel of ten T cell markers confirmed that VXN *in vivo* treatments were effective at inducing T cell infiltration in CT26 tumors (**Figure 8C**). Overall, these results indicate that VXN treatments are effective at reactivating retroelements expression, which, in turn, stimulate an immune antiviral response in CRC cells. Additionally, mice treated with VXN showed significantly smaller tumor size compared to mice treated with saline control (data not shown). Such a pharmacological tool stimulating LINE1 and hERV expression represents an interesting avenue to create an "immune hot" tumor microenvironment in CRC.

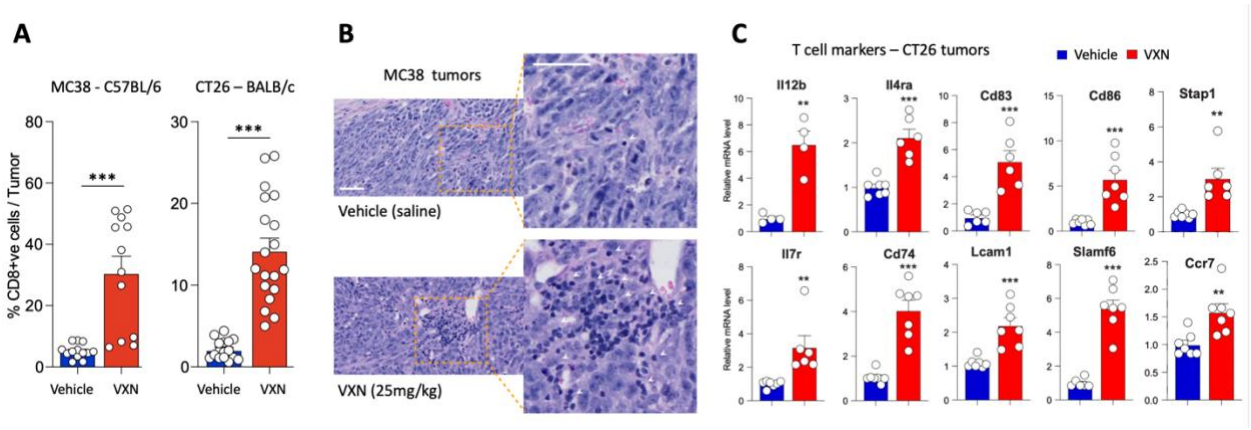

Figure 8 – **Increase in T cell infiltration in mouse tumors treated with VXN. A)** High-content imaging analysis of CD8 immunofluorescence staining on MC38 (n≥12) and CT26 (n≥13) tumors treated with VXN and saline. The percentage of CD8-positive cells (green) is presented for each model/condition (***: ≤0.0001, *: p=0.0449, one-way ANOVA). **B)** Representative pictures of hematoxylin and eosin staining showing lymphocyte infiltration in VXN-treated CRC tumors vs. vehicle controls. Tissue sections were analyzed by a certified pathologist, and white arrowheads indicate the presence of lymphocytes (n=3 independent tumor pairs, scale bar: 50 µm). C) qPCR analysis of a panel of ten T cell markers in bulk CT26-BALB/c tumors excised from vehicle and VXN-treated mouse primary recipients (n=6 from 3 independent tumor pairs, ***: ≤0.0005, **: ≤0.0055).

4.2 Objective 2: To develop new tools to downregulate transposable elements mobility in colorectal cancer

Given that LINE-1 retrotransposition levels have been shown to be involved in CRC tumorigenesis and L1ORF1p RMM-CTD domains represent potential druggable targets to disrupt the LINE-1 cycle, the discovery of new compounds that interact with L1ORF1p hold the potential to prevent the early onset of CRC as well as the progression of the disease.

To screen for novel high-affinity disruptors of L1ORF1p functions, we used a docking-based *in silico* approach. Virtual high-throughput chemical screening, conducted in collaboration with Muhammad Shah (former lab student), was performed using the Drugbank virtual library. A total of 9,181 compounds in 3D structure format were screened, and 49 candidates exhibited binding energy (ΔG) of $\leq$ -9 kcal/mol with the RMM-CTD domains of L1ORF1p (PDB #2LDY). The Pan-Assay Interference compounds filter (PAINS) was then applied to these 49 candidates to identify false positive drugs [136], and all 49 compounds passed the filter. Among these candidates, 46 are commercially available, of which 11 are FDA-approved for clinical use (**Figure 9A**). Within the 11 candidates, 5 are approved for treating migraines, 3 for metastatic cancer, 1 for benign hyperplasia, 1 for hyponatremia, and 1 as an antiparasitic. The abundance of hits impacting molecular mechanisms associated with one specific condition, migraine, led us to prioritize compounds from this subgroup in subsequent experiments. Ubrogepant and Dihydroergotamine both prevent migraines, however through two different mechanisms.

Once the drug candidates were chosen, PERMM analysis of the L1ORF1p inhibitor candidates demonstrated that both compounds can passively permeate through the cellular membrane (**Figure 9B**).

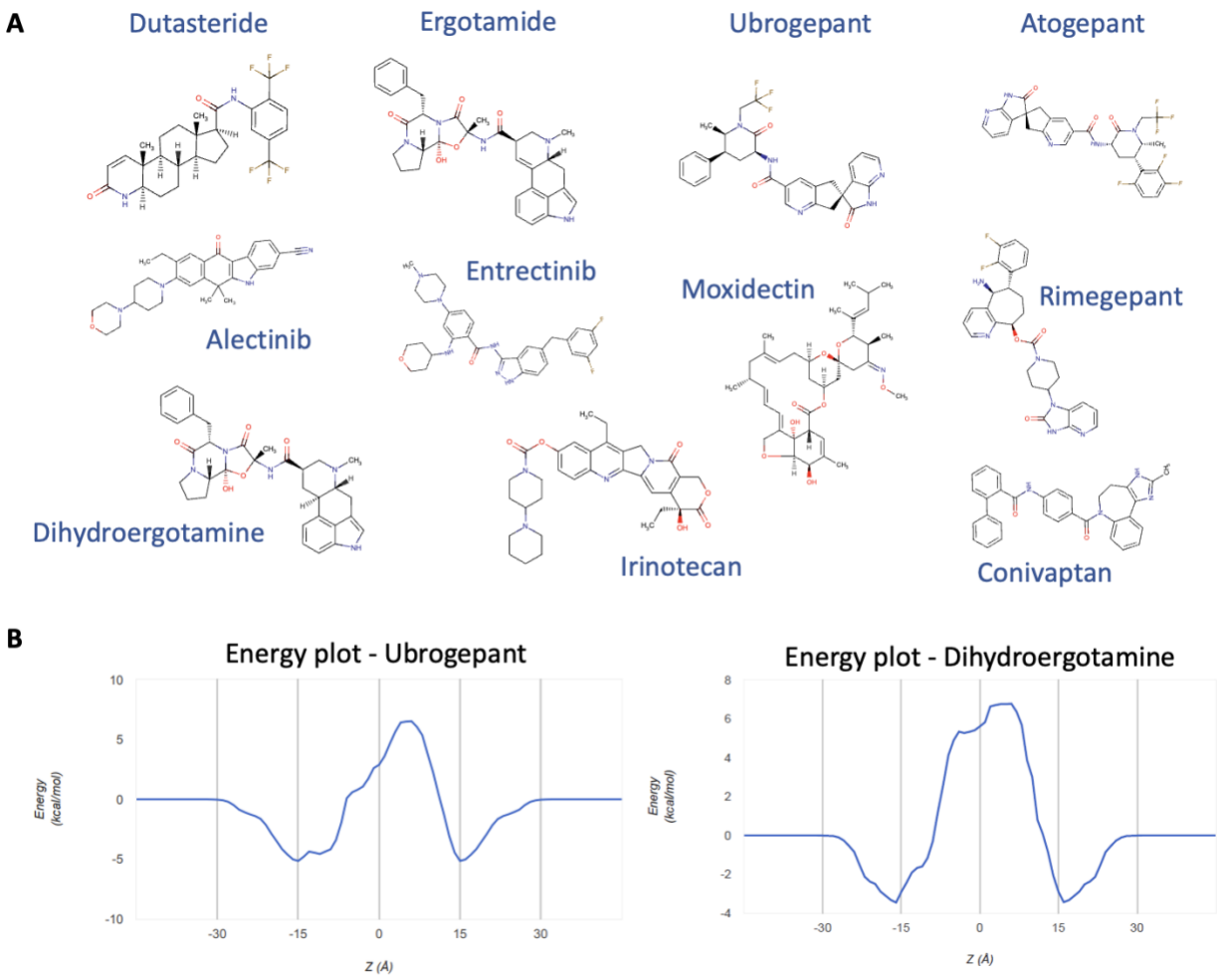

Figure 9 – Chemical structures of main candidates and energy plots of the two lead compounds. A) Chemical structures of the 11 FDA-approved compounds, identified by the *in silico* drug screening, that interact with RMM-CTD domains of L1ORF1p. **B)** Energy plots of Ubrogepant (left) and Dihydroergotamine (right).

Based on our *in silico* docking results, 2D ligand-protein diagrams were generated using LigPlot+ to visualize the predicted interactions between the drug candidates and the amino acids of L1ORF1p RNA binding domains (**Figure 10A**). 3D docking schematics show different binding pockets for each drug candidate, all of which exhibit negative and similar binding energy scores, indicating a high likelihood of those compounds interacting with the target protein (**Figure 10B**).

Dose-response assays were performed in HIEC, HCT116, HT29, and HeLa cells to evaluate the impact of these candidates on growth rates. The analysis was conducted using high-content imaging normalized to the DMSO control (**Figure 10C**). Previous publications have shown that the doses used to treat cell lines are in the nanomolar range [137, 138]. In general, both compounds did not demonstrate significant toxicity to the cell lines.

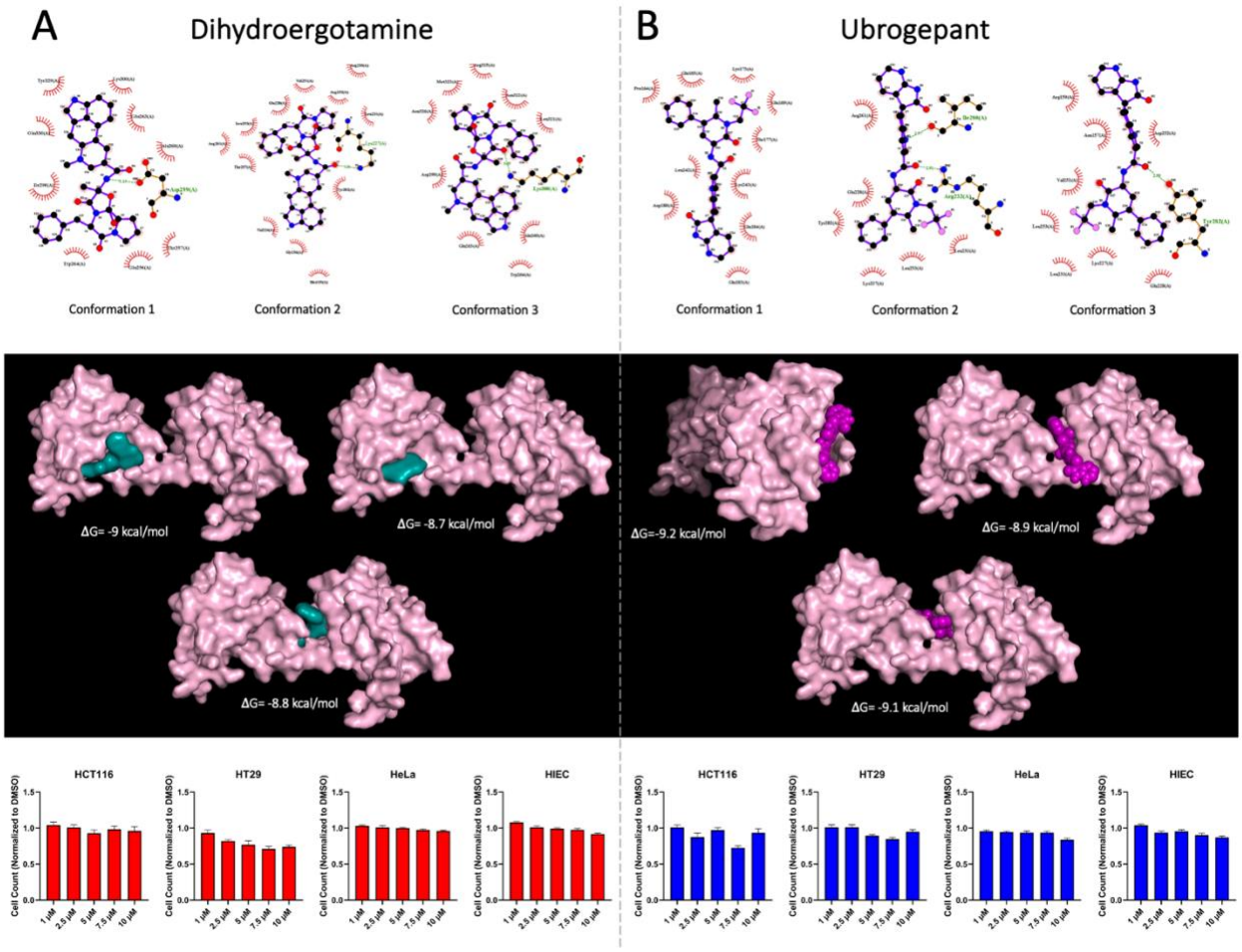

Figure 10 – Structural prediction of Dihydroergotamine and Ubrogepant binding to the L1ORF1 RNA binding domains and dose-response experiment. A) 2D representation of the predicted binding pocket of Dihydroergotamine and Ubrogepant in the RMM-CTD domains of L1ORF1p (black, carbon; red, oxygen; blue, nitrogen; pink, fluorine). Dashed lines represent the predicted hydrogen bond lengths (Å). **B)** Predicted 3D docking images of the L1ORF1 inhibitors candidates, Dihydroergotamine and Ubrogepant, bound to the RMM-CTD domains of L1ORF1p. Each compound binds to the target in three different pockets with varying binding energy scores. **C)** Dose-response experiment assessing the growth of HCT116, HT29, HeLa, and HIEC cultures following Dihydroergotamine and Ubrogepant treatments (72 h, 1-10 μM, n=3).

In parallel to the virtual drug screening, I investigated the expression levels of L1ORF1p, in a range of cell lines, including t-hESC, HIEC, SW480, HT29, HCT116, HeLa, and HEK293T. According to previous study [139], the higher the expression of L1ORF1p, the more aggressive or stem-like the cell line is. Therefore, transformed human pluripotent stem cells (t-hESC) were used as a positive control for this experiment. HIECs, as human normal intestinal epithelial crypt cells, were used as a negative control. The measurements were taken from cell lysates by Western blot (**Figure 11A**). To further study the expression of L1ORF1p, I performed Western blot analysis of ground tissue from colorectal tumors and their adjacent normal tissues from five different CRC patients (**Figure 11B**).

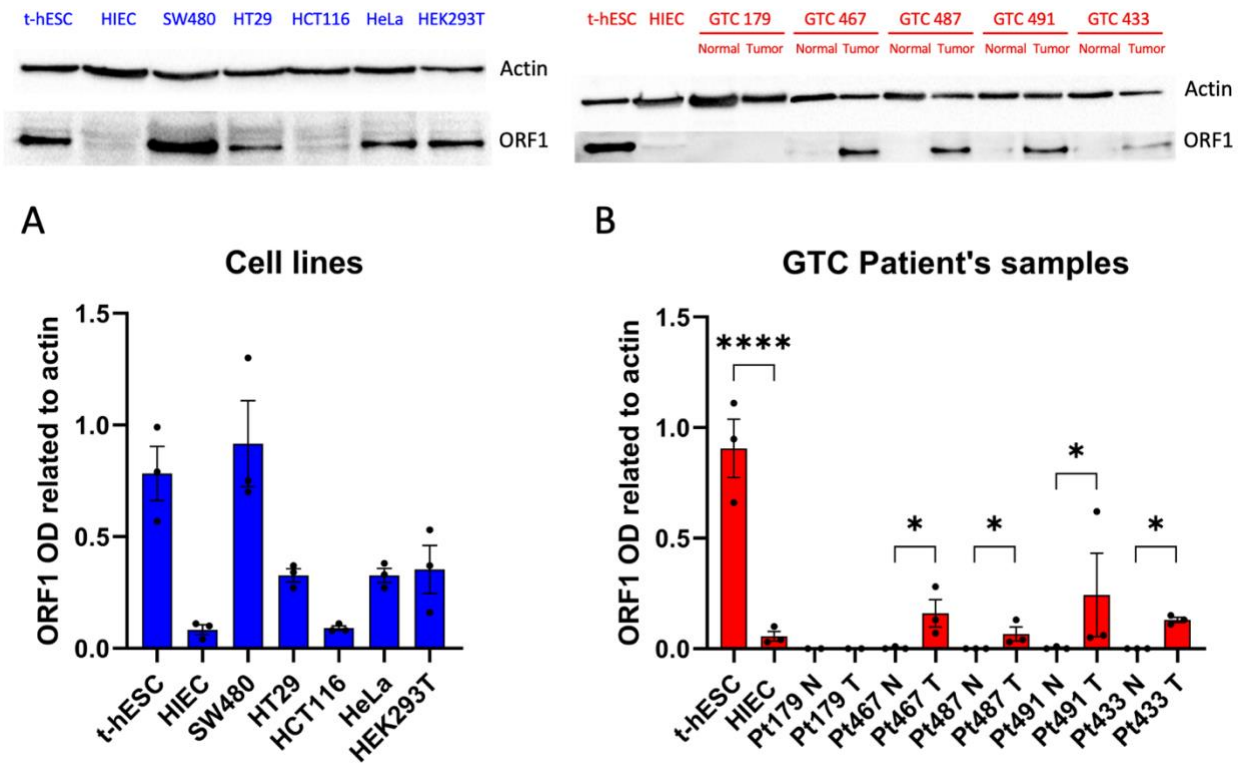

Figure 11 – L1ORF1p expression levels. A) L1ORF1p (41kDa) expression levels in different cell lines, including transformed embryonic stem cells (h-hESC), normal intestinal epithelium cells(HIEC), CRC cell lines (SW480, HT29, and HCT116), and other types of cancer cell lines (HeLa and HEK293T), n=3. **B)** L1ORF1p expression levels in five sets of CRC patient samples (normal colon and tumor tissues), n=3 (****, $p < 0.0001$; *, $p \leq 0.05$).

In line with previous literature, where stem-like cells express higher levels of L1ORF1p, t-hESC cells showed high levels of L1ORF1p expression, and HIEC cells showed low levels. Consistently, CRC cell lines SW480, HT29 and HCT116 expressed higher levels of L1ORF1p at various levels compared to HIECs (**Figure 11A**). Human cervical cancer-derived HeLa cells also showed higher L1ORF1 protein levels than HIEC cells (**Figure 11A**). L1ORF1 protein levels were low in normal colonic samples, and could not be detected in certain extracts even after a long exposure of the blot membrane. In contrast, L1ORF1p was detectable in the extract of colorectal tumor tissue in four out of five patients. Taken together, these results suggest that LINE-1-encoded L1ORF1p are more expressed in colorectal tumor tissues, regardless of patient-dependent variance. Given that L1ORF1p is required for the process of LINE-1 retrotransposition activity, which could potentially increase genomic instability, characterizing the expression patterns of these proteins may possibly serve as one of the factors responsible for genome instability in these cells.

Beyond the identification of protein expression in cancer versus normal settings, including cell lines and CRC patient-derived samples, it is important to understand the differences at a cellular level, such as the localization of this protein during periods of increased retrotransposition events. A recent study in breast cancer reported that nuclear localization of L1ORF1p was significantly associated with aggressive behavior of cancer and poor outcome [139]. To address these findings in colorectal cancer, the subcellular localization of L1ORF1p was investigated in colorectal cancer cell lines treated with drugs that increase retrotransposable elements activity and analyzed by immunocytochemistry (**Figure 12**). The results show that when the cells are treated with compounds that reactivate the LINE-1 retrotransposons, 5AZA and VXN, there is an increase

in the nuclear levels of L1ORF1p. The nuclear translocation of L1ORF1p could be associated with higher levels of retrotransposition events, as the reinsertion step takes place in the nucleus.

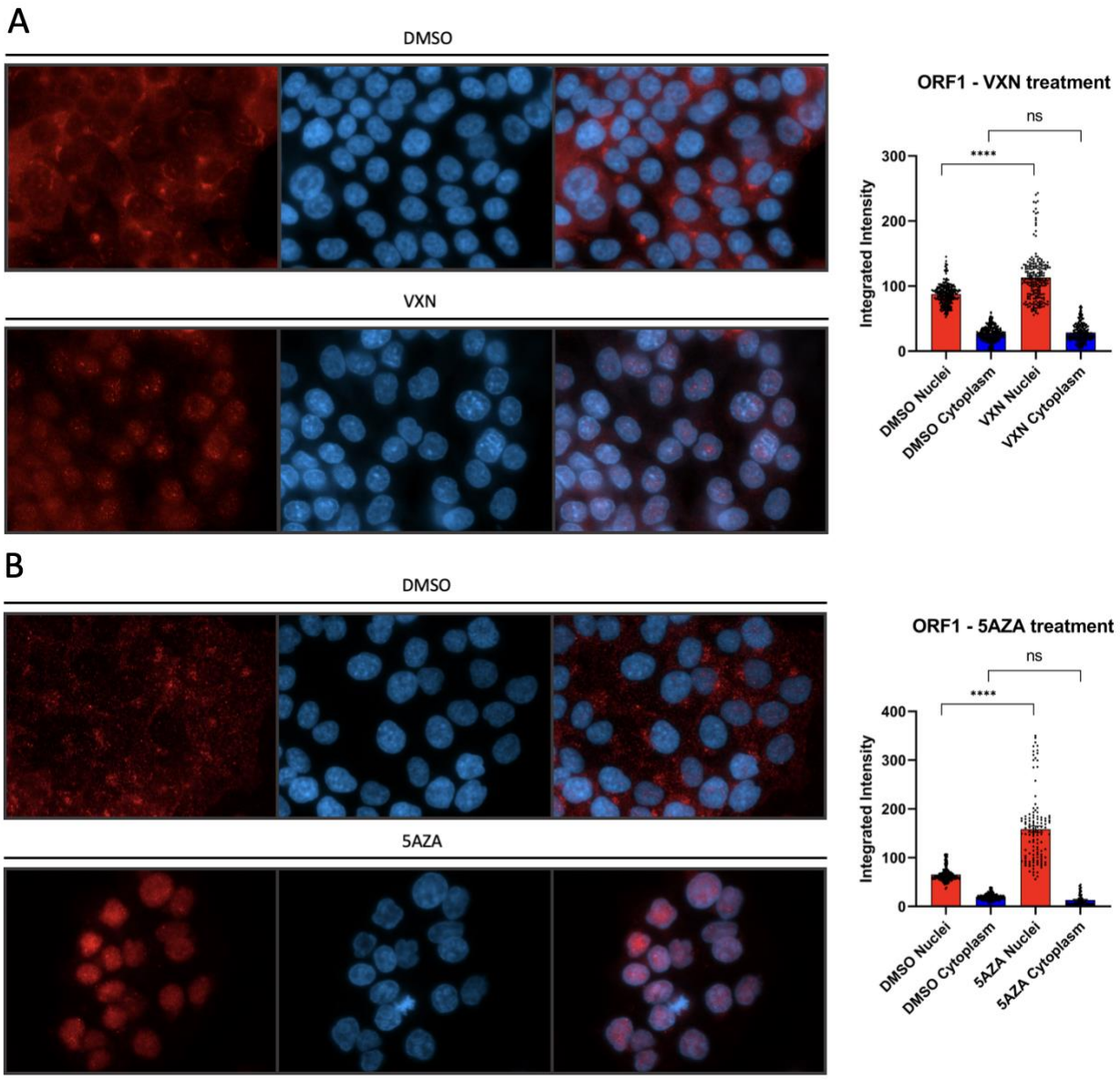

Figure 12 – L1ORF1p subcellular localization in HCT116 treated with VXN and 5AZA. A) HCT116 cells treated with VXN and DMSO as a control, stained with DAPI in blue, L1ORF1p in red. **B)** HCT116 cells treated with 5AZA and DMSO as a control, stained with DAPI in blue and L1ORF1p in red, (n=3, ****: $p<0.0001$).

To study the subcellular localization of L1ORF1p upon drug treatments, cells were treated with 5AZA in combination with the L1ORF1 inhibitor candidates to assess if the nuclear translocation of L1ORF1p is reduced. Dihydroergotamine and Ubrogepant significantly decreases the nuclear translocation of L1ORF1p in HCT116 cells induced by cotreatment with 5AZA for 72 hours (**Figure 13**). Treating the cells alone with the L1ORF1 inhibitor candidates, no significant change in L1ORF1 subcellular localization is seen (data not shown). Critically, these results demonstrate a rescue effect of those two compounds in halting the nuclear translocation of L1ORF1p, counteracting the induction of expression and nuclear localization caused by DNA demethylation through 5AZA treatment.

After demonstrating the impact of drug treatments on L1ORF1p subcellular localization, indicating a connection between nuclear translocation of L1ORF1p and its activity, a LINE-1 reporter construct activated upon de novo integration was used to examine the influence of our lead compounds on LINE-1 retrotransposition levels (**Figure 14**). Following transfection of HCT116 cells with this reporter system, the cells that successfully complete a full LINE-1 retrotransposition cycle will express eGFP.

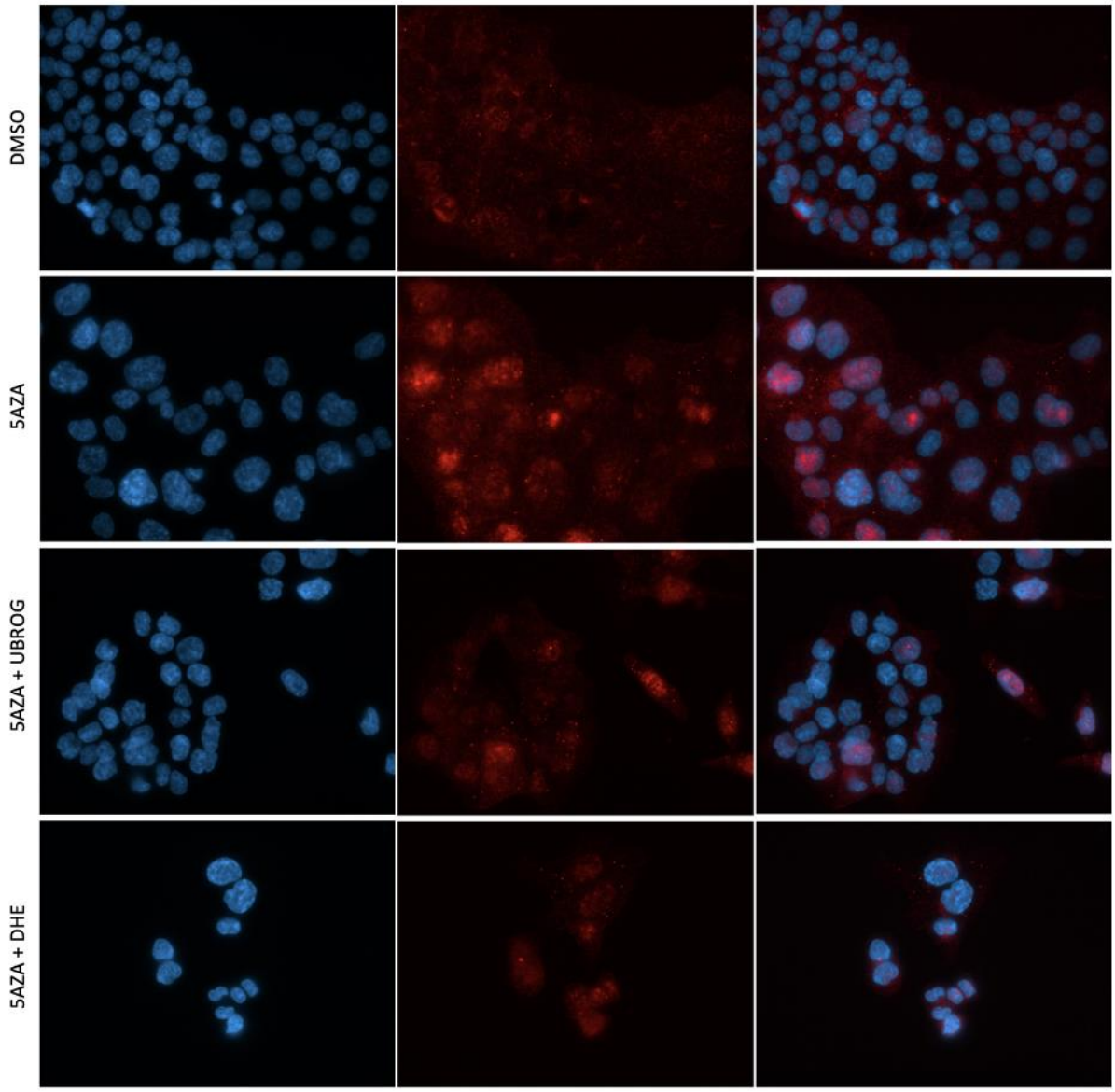
DMSO
5AZA
5AZA + UBROG
5AZA + DHE

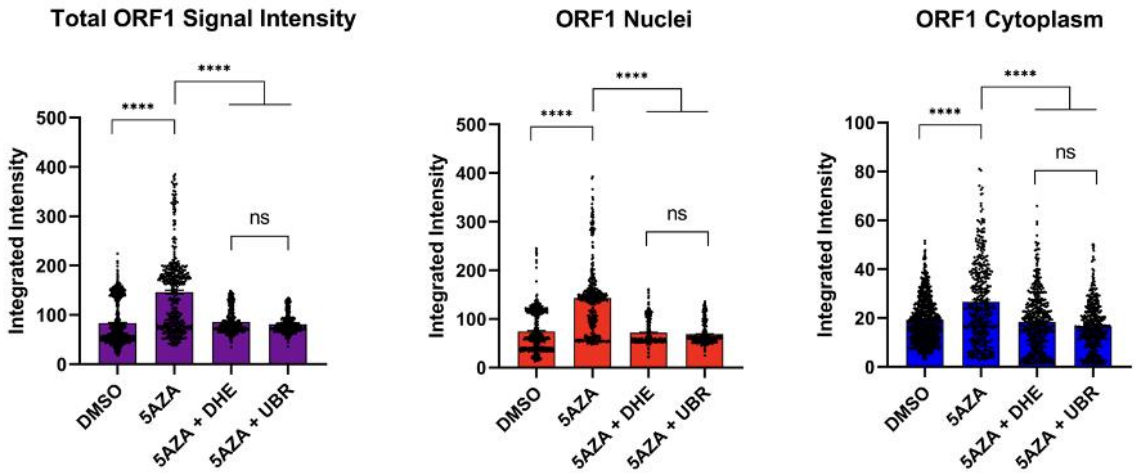
Total ORF1 Signal Intensity
ORF1 Nuclei
ORF1 Cytoplasm
Integrated Intensity
****
ns
DMSO
5AZA
5AZA + DHE
5AZA + UBR

Figure 13 – L1ORF1p subcellular localization in HCT116 treated with inhibitor candidates. HCT116 treated with 5-Azacitidine (3 μM) alone and co-treated with Dihydroergotamine (4 μM) and Ubrogepant (4 μM), compared to DMSO (72 h, ****: p<0.0001), n=3. DMSO versus both combinations 5AZA+DHE and 5AZA+UBR shows non-significant statistical differences in all 3 graphs. Red: L1ORF1p (Alexa 647). Blue: nuclei (DAPI). Images were obtained at 63x magnification, and subcellular quantification was analyzed with Cell Profiler.

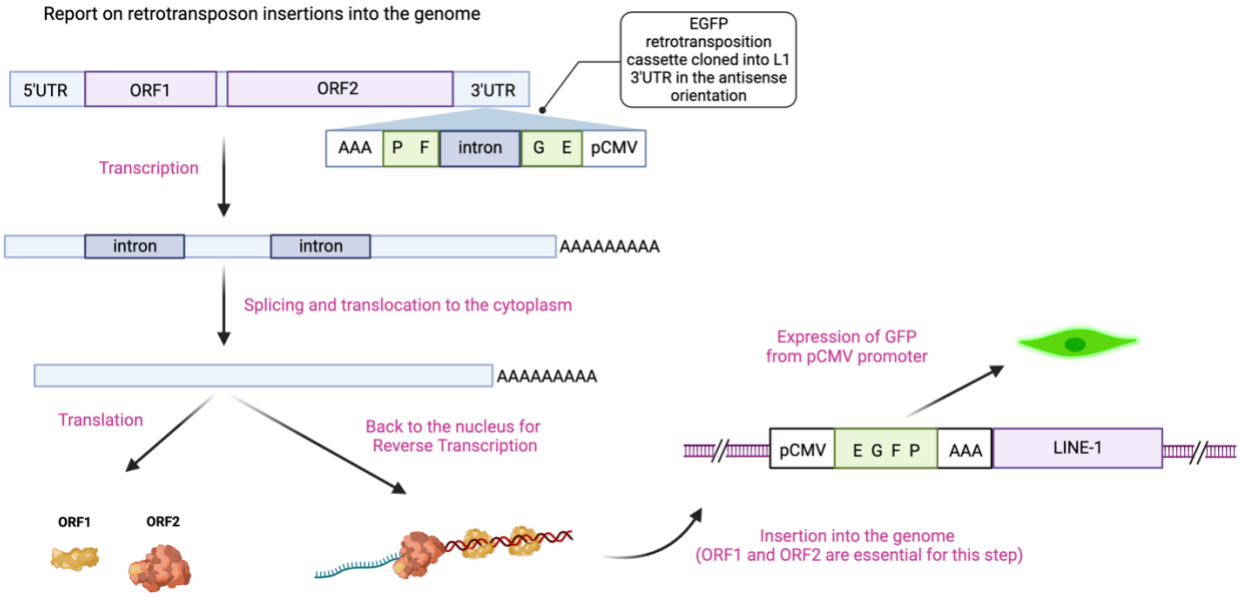

Figure 14 – LINE-1 reporter assay. A) Schematic of the LINE-1 reporter system. Schematic created with BioRender.com.

To determine whether DHE and UBR can block the LINE1 retrotransposition cycle in CRC cells, I used HCT116 cells transduced with the LINE-1 retrotransposition reporter which I treated with 5AZA, DHE, or UBR alone, and combinations of DHE+5AZA or UBR+5AZA (**Figure 15**). The number of GFP-positive cells was quantified using high-content imaging and compared between the different treatments as well as DMSO controls. As expected, cells treated with 5AZA exhibit increased LINE-1 RT levels, however, no significant changes were observed in LINE-1 reporter activity in cells treated with 5AZA and both L1ORF1p inhibitor candidates versus 5AZA alone. Additional experimental replicates could be performed to validate this conclusion. Despite their ability to modulate L1ORF1 protein levels and subcellular distribution, my data suggest that DHE and UBR do not effectively block *de novo* integration of LINE-1 elements in the genome of human CRC cells.

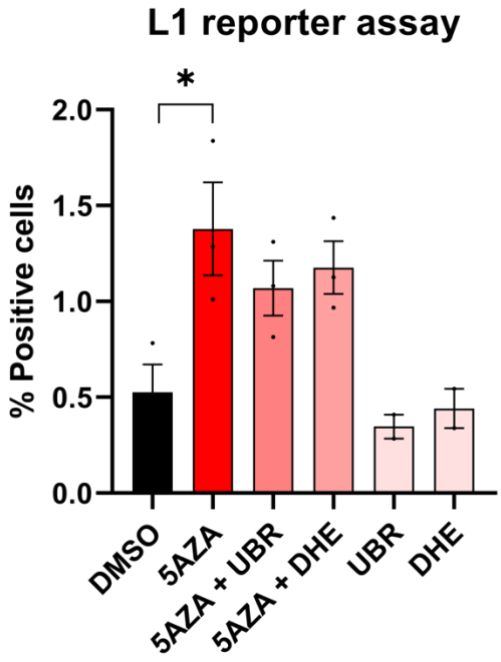

Figure 15 – Retrotransposition levels in HCT116s treated with lead candidates. HCT116 cells transfected with the LINE-1 reporter, selected with puromycin, and treated for 72 hours with 5-Azacitidine (5AZA, 3 μM) and/or L1ORF1 inhibitor candidates: Dihydroergotamine (DHE, 4 μM) and Ubrogepant (UBR, 4 μM), n=3, $p \leq 0.05$.

4.3 Objective 3: Establishment of colonic organoids derived from healthy tissues as a normal counterpart tool to study the toxicity of new drug candidates

Recently, cancer organoids have become a widely used model in cancer research due to their disease-modelling advantages over 2D cultures of standard cancer cell lines. Growing cancer cells as organoids yields a better representation of the architecture and functionality of a tumor and can recapitulate certain aspects of the tumor cellular heterogeneity.

Specifically in colon organoids, these structures initially expand into monolayered spheres and then can exhibit crypt-like protrusions resembling the glandular epithelium found in the original tissue. Thanks to their ability to maintain stem cells, colon organoids can be continuously expanded, offering an exceptionally valuable source of untransformed primary cells [140].

In previous work conducted in our lab, we established a protocol for serial tumor organoid plating, using primary CRC tissues to investigate the impact of small molecules on the CCSC [141]. Now, we have developed a protocol for patient-derived normal colonic organoids using crypts harvested from the healthy colon tissue adjacent to the tumors resected from CRC patients (**Figure 16**). This model is a powerful tool for our research as it allows us to use the matching normal counterpart of the tumor sample as a control in our experiments.

As previously stated, normal tissue samples are collected from the Global Tissue Consenting and Collecting Program (GTC) in collaboration with The Ottawa Hospital. As soon as the human healthy colon tissue is received, the sample processing starts immediately. This last chapter of my thesis consists of a technical resource that I established during my master's and is presented as a step-by-step protocol. This achievement now provides the Benoit lab with a powerful system to test drug candidates, including putative LINE-1 modulators, for their capacity

to target vulnerability points in CRC cells while simultaneously assessing their impact in normal colonic tissues.

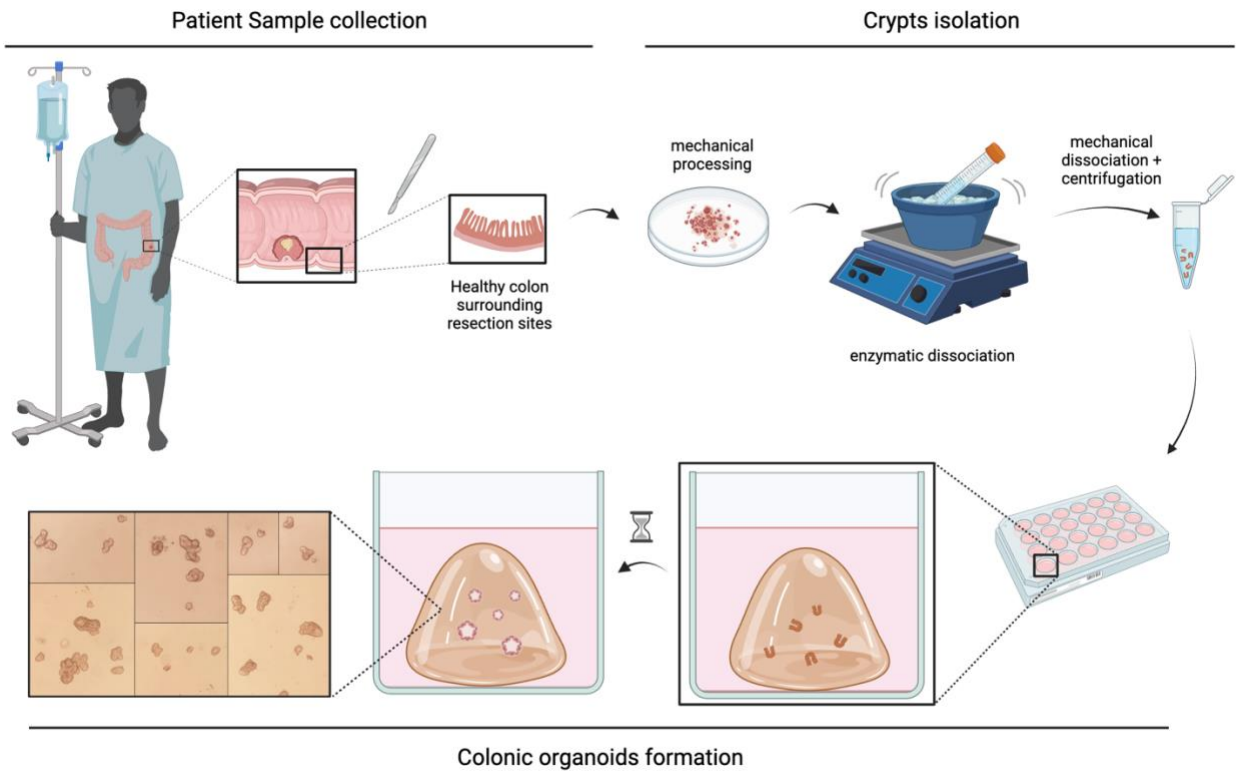

Figure 16 – Schematic of the method used to establish colonic organoids from primary human healthy colon samples. Healthy colon tissue surrounding resection sites is collected from CRC patients, and samples are quickly processed. The tissue undergoes mechanical processing, followed by enzymatic digestion on ice and mechanical dissociation, causing crypts to detach from the submucosa tissue layer. After centrifugation and washing steps, the isolated crypts are mixed with BME and seeded as 3D-domes organoids. The stem cells present in the colon crypts recapitulate the original structures, giving rise to colonic organoids. These organoids serve as counterparts of colorectal cancer tumor organoids. Created with BioRender.com.

4.3.1 Human colonic organoids crypts isolation protocol

1. Obtain a freshly resected colon sample in a 50 mL collection tube on ice, and immediately proceed to tissue dissociation in a biological safety cabinet.
2. Place the following reagents on ice: PBS without Ca^{2+} and Mg^{2+} (sterile PBS with EDTA 2 mM) and DMEM/F-12 with 15 mM HEPES + 1% BSA.
3. Place a tissue culture-treated 24-well plate in a 37°C incubator for at least 30 minutes.
4. In a 50 mL conical tube, wash the tissue sample obtained from colon biopsies with 20 mL of ice-cold PBS without Ca^{2+} and Mg^{2+}. Allow the tissue to settle by gravity, then aspirate the supernatant.
5. Repeat step 3 two more times, leaving 1 mL of supernatant in the tube.
6. Transfer the tissue to a 10 cm dish. Using sterile scissors, thoroughly mince the tissue into the smallest pieces possible. Rinse a 15 mL conical tube with ice-cold PBS without Ca^{2+} and Mg^{2+}. Use scissors to cut the aspirating end of a p1000 tip to make it wider, pre-wet the tip with PBS, and use it to transfer the minced tumor fragment suspension to the pre-rinsed conical tube.
7. Allow the tissue fragments to settle by gravity (~ 5 seconds), then aspirate supernatant.
8. Add 10 mL of Corning® Cell Recovery Solution, then incubate on ice on a rocking platform set at medium speed (~ 40 rpm) for 30 minutes.
9. Centrifuge at 290 x g for 5 minutes. Aspirate supernatant.

Note: For the remainder of the protocol, pre-wet pipette tips with DMEM/F-12 with 15 mM HEPES + 1% BSA before manipulating the tissue sample. This prevents crypts from sticking to the wall of the pipette tip.

10. Add 1 mL of ice-cold DMEM/F-12 with 15 mM HEPES + 1% BSA. Again, use scissors to cut the end of a p1000 tip and vigorously pipette up and down 20 times with a 1 mL pipette to remove crypts from tissue.

    Note: Avoid touching the side/bottom of the tube with the pipette tip. This tube contains isolated crypts that can be used for establishing colonic organoid culture.

11. Place 20 µL of the crypt suspension in a 10 cm dish and visualize at the microscope to ensure there are at least 5 crypts.

    Note: At this point, take an aliquot of basement membrane extract (BME) (e.g., Matrigel®) from -80°C and let it thaw on ice. For 6 domes, a 150 µL aliquot of BME is sufficient. Remove the complete IntestiCult™ Organoid Growth Medium from the -80°C freezer and let it thaw at room temperature (15-25°C). Once it is thawed, add a combination of the following antibiotics: PenStrep (100 U/mL final concentration) and Amphotericin B (1 µg/mL final concentration).

12. In a sterile microtube, add the same volume of crypt suspension (e.g., 300 µL).
13. Once the BME aliquot has completely thawed, quickly add BME to the crypt suspension according to a 1:1 ratio (BME:crypt suspension). Gently homogenize the BME/crypt mixture. Avoid introducing bubbles.
14. In the pre-heated 24-well plate, carefully deposit 50 µL of the mixture at the center of each well to form dome structures. To prevent bubbles when plating, dispense to the first stop of the pipette.

    Note: Proceed quickly to ensure BME does not polymerize before dome formation.

15. Without disrupting the domes, place the lid on the culture plate and gently transfer it to the incubator for a 10-minute incubation at 37°C, 5% CO_2. Ensure to transfer the plate very steadily without tipping or using swift movements.
16. Once the polymerization period is over, transfer the dome-containing plate back to the biological safety cabinet. Ensure BME domes have preserved their integrity and have not dispersed across the well.
17. Fill the dome-containing wells with 500 µL room temperature (15-25°C) complete IntestiCult™ Organoid Growth Medium by pipetting the medium gently down the sidewall of the well. Do not pipette the medium directly onto the domed cultures.
18. Add sterile PBS to all unused wells to ensure proper hydration of the cultures.
19. Place the lid on the culture plate and incubate at 37°C and 5% CO_2.
20. Monitor cultures for organoid growth. Typically, by day 4 crypts start budding and growing in size in the next couple of days. After the first passage, small cystic organoids will begin to appear and grow in size as well.

    Note: The size and survival rate of the initial crypts are patient dependent.
21. Fully exchange the culture medium three times per week by carefully aspirating the existing liquid medium, keeping the pipette tip at the edge of the well bottom. Replace with 500 µL fresh, room temperature complete IntestiCult™ Organoid Growth Medium.

    Note: After 7 to 10 days organoids should be fully formed and ready to be passed. Each well can be split into 3 to 4 wells. Normal colonic organoids should be split at least once before any drug treatment or other experiments.

On average, the minimum time required to obtain long-term colonic organoids culture is 14 days. It is also important to prevent the organoids from overgrowing (**Figure 17**).

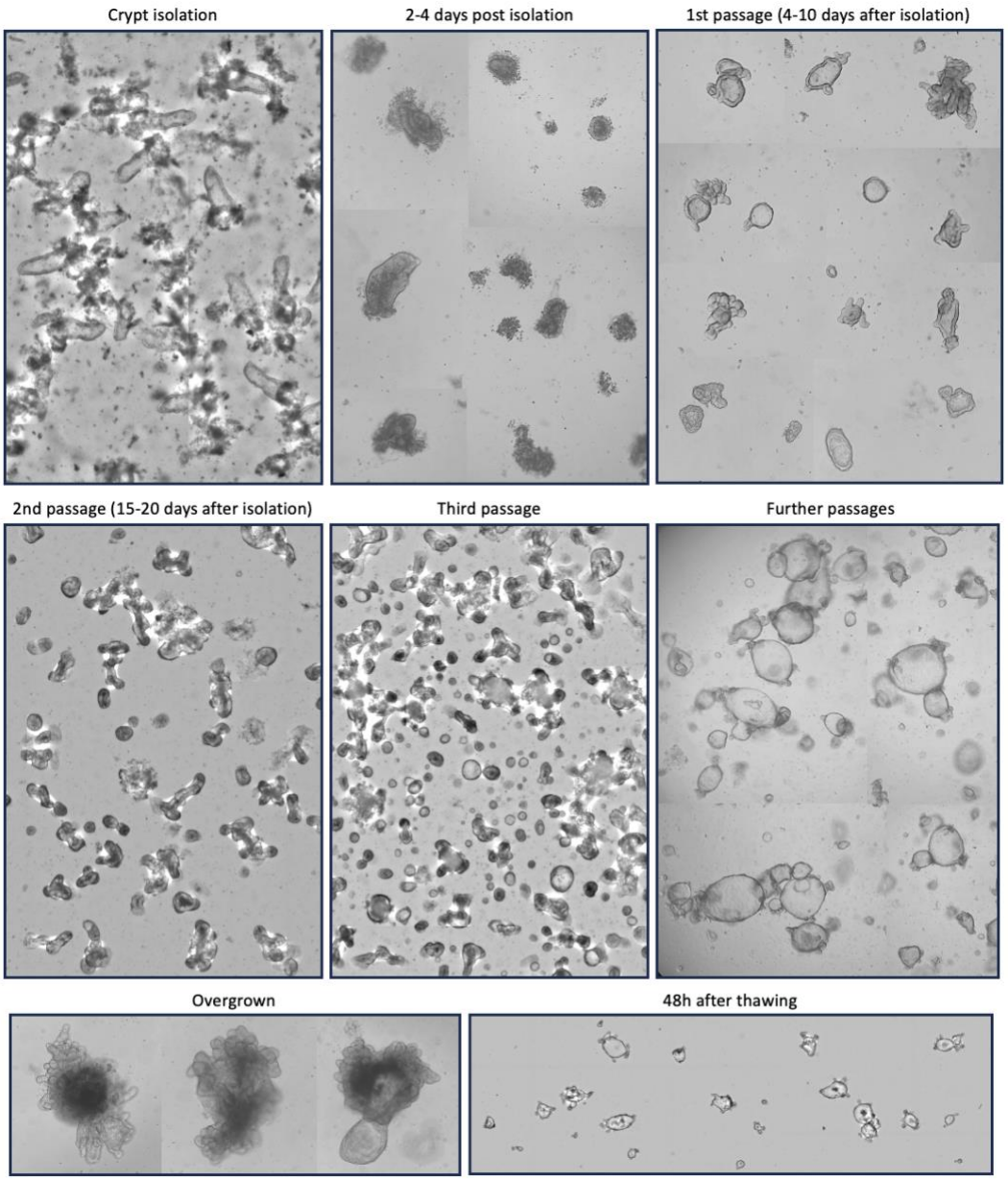

Figure 17 – Schematic representation of the experimental workflow from crypt isolation to 3D organoids generation. The initial phase of growth, transitioning from crypts to organoids, takes approximately 10-15 days. Splitting step can be repeated multiple times, depending on the experimental design. If desired, the cultures can be preserved through cryopreservation for later use and to generate a biobank of patient-derived samples.

4.3.2 Human colonic organoids passage protocol

1. Remove complete IntestiCult™ Organoid Growth Medium from the fridge or freezer and leave to warm to room temperature (15-25ºC). Place Gentle Cell Dissociation Reagent and DMEM/F-12 with 15 mM HEPES on ice. Place the required number of tissue culture-treated 24-well culture plates at 37ºC to pre-warm for 30 minutes.
2. Gently aspirate the media from each well without disturbing the domes.
3. Add 1 mL of ice-cold Gentle Cell Dissociation reagent on top of the exposed dome in each well to chemically dissociate the BME domes and organoids. Incubate at room temperature (15-25ºC) for 1 minute.
4. Pre-wet a p1000 tip with the Gentle Cell Dissociation Reagent and break up the dome and organoids by pipetting up and down approximately 10 times or until all the Matrigel® has been dissolved. Repeat that process for each well.
5. Use the same pipette tip to transfer the suspension to a 15 mL conical tube. Rinse the culture well with an additional 1 mL Gentle Cell Dissociation Reagent and add this to the same 15 mL tube.

   Note: Crypts are likely to stick to the walls of the tube. To avoid that, pre-wet the tube with Gentle Cell Dissociation Reagent.
6. Repeat steps 4 and 5 for each well to be passaged.
7. Incubate the 15 mL tubes at room temperature (15-25ºC) on a rocking platform at 20 rpm for 10 minutes.

   Note: At this point, take an aliquot of BME (e.g., Matrigel®) from -80ºC and let it thaw on ice. A 100 µL aliquot of BME per each well to be passaged is sufficient.

8. Centrifuge the tubes at 4ºC and 290 x g for 5 minutes, then gently pour off and discard the supernatant.
9. Wash the pellets by resuspending in 10 mL ice-cold DMEM/F-12 using a pre-wetted 10 mL serological pipette, and re-centrifuge the suspension again at 4ºC and 200 x g for 5 minutes.
10. Gently pipette off as much DMEM/F-12 as possible without disturbing the pellet and discard the supernatant.
11. Add 100 µL room temperature (15-25ºC) complete IntestiCult™ Organoid Growth Medium to the pellet in each tube. Add 100 µL undiluted BME to each tube and pipette up and down 10 times to resuspend the pellet. Avoid introducing bubbles.
12. For each tube, carefully pipette 50 µL of the medium/BME suspension into the center of each of 4 wells of a pre-heated 24-well plate to form domes. To prevent air bubbles when plating, dispense to the first stop of the pipette.

    Note: Proceed quickly to ensure BME does not polymerize before dome formation.
13. Without disrupting the domes, place lid on the culture plate and gently transfer it to the incubator for a 10-min incubation at 37ºC, 5% CO_2. Ensure to transfer the plate very steadily without tipping or using swift movements.
14. Once the polymerization period is over, transfer the dome-containing plate back to the biological safety cabinet. Ensure BME domes have preserved their integrity and have not dispersed across the well.
15. Fill the dome-containing wells with 500 µL room temperature (15-25ºC) complete IntestiCult™ Organoid Growth Medium by pipetting the medium gently down the sidewall of the well. Do not pipette the medium directly onto the domed cultures.

16. Add sterile PBS to all unused wells to ensure proper hydration of the cultures.
17. Place the lid on the culture plate and incubate at 37°C and 5% CO_2.
18. Exchange the culture medium 3 times per week by carefully aspirating the existing liquid medium, keeping the pipette tip at the edge of the well bottom. Replace with 500 µL fresh, room temperature (15-25°C) complete IntestiCult™ Organoid Growth Medium.

4.3.3 Human colonic organoids cryopreservation protocol

For optimal results, cryopreservation is best performed 3 to 4 days after passage, when organoids are in exponential growth phase.

1. Remove complete IntestiCult™ Organoid Growth Medium from the fridge or freezer and leave to warm to room temperature (15-25°C). Place PBS without Ca^{2+} and Mg^{2+} and complete DMEM/F-12 (15 mM HEPES, GlutaMAX™ 1x, PenStrep 100 U/mL) and Freezing media on ice. Label the required cryovials before starting the protocol.

   Note: Freezing medium is composed of complete IntestiCult™ with 10% DMSO and 40% KnockOut™ Serum Replacement.
2. Retrieve from the incubator the plate containing the organoids that are being cryopreserved. Using an inverted microscope, count the number of organoids found in each well. Combine the contents of multiple wells as needed to achieve 200 organoids per cryovial to be filled.
3. Carefully aspirate the entire volume of medium from each well containing organoids. Replace it with 1 mL of complete DMEM/F-12 medium.
4. Break up the BME by pipetting up and down 2-3 times with a pre-wetted p1000 tip. Transfer suspensions containing 200 organoids to 15 mL conical tube.

5. Wash each well with 1 mL of complete DMEM/F-12 medium by pipetting up and down 2-3 times with a pre-wetted p1000 tip and transfer to the 15 mL conical tube.
6. Pellet the organoids by centrifuging at 290 x g for 5 minutes at 4°C. Carefully remove and discard the supernatant. To avoid aspirating the organoid pellet, remove the last 1 mL of medium by using a pre-wetted p1000 tip followed by a pre-wetted p200 tip.

   Note: Verify if there is no BME left, without disrupting the pellet. If some BME is left, resuspend the pellet with complete DMEM/F-12 medium and centrifuge the tube again. Completely remove the supernatant without disrupting the pellet.
7. Gently resuspend organoid pellet using 1 mL of ice-cold freezing medium per cryovial of 200 fragmented organoids. Ensure slow addition of freezing medium to avoid an osmotic shock to the cells. Pipette up and down approximately 25 times, in order to fragment them prior to cryopreservation.

   Note: Intact organoids may still be present if too little pipetting was performed. If too much pipetting was performed, an excess of single cells and debris may be observed. Cystic organoids fragment more rapidly than budded organoids.
8. Using the same pipette tip, transfer 1 mL of the fragmented organoids suspended in freezing medium to each labeled cryovial. Place the cryovial in a freezing container with 500 mL of isopropyl alcohol.
9. Immediately transfer the freezing container to a -80°C freezer for 24 hours then transfer the cryovial to liquid nitrogen (-135°C) for long-term storage. Long-term storage at -80°C is not recommended.

   Note: Work quickly to avoid prolonged exposure of non-frozen organoids to freezing medium.

4.3.4 Human colonic organoids thawing protocol

1. Place 150 µL of BME on ice and let complete IntestiCult™ Organoids Growth Medium warm to room temperature (15-25ºC). Place a 24-well tissue culture-treated place in an incubator at 37ºC to warm up for 30 minutes.
2. Prepare a DMEM/F-12 washing solution with 1% BSA and 15 mM HEPES. Leave at room temperature (15-25ºC) for the duration of this protocol. The washing solution can be stored at 4ºC for up to 6 months.
3. To a 15 mL conical tube add 2 mL of DMEM/F-12 washing solution at room temperature.

   Note: Cells should be transferred to this tube immediately after thawing to avoid significant reduction in viability.
4. Thaw frozen organoids by placing the cryovial in a 37ºC water bath. Thawing is complete when the freezing medium becomes liquid, at which point the organoids will be visible at the bottom of the tube.

   Note: Thawing at 37ºC should take between 2 and 2.5 minutes; over-warming the medium may affect the growth efficacy of the organoids in culture.
5. Wipe the outside of the cryovial with 70% ethanol or isopropanol before opening. Add 1 mL of DMEM/F-12 washing solution directly to the cryovial. Mix the contents of the cryovial by pipetting up and down 4 times. Immediately transfer the contents of the cryovial to the 15 mL conical tube containing 2 mL of DMEM/F-12 washing solution using a pre-wetted p1000 tip.
6. Wash the cryovial 1 more time with 1 mL of DMEM/F-12 washing solution and transfer to the conical tube. Be sure to wash the entire inner surface area of the cryovial, including the inside of the lid.

7. Centrifuge the organoid suspension at 200 x g for 5 minutes at 4°C. Carefully remove and discard the supernatant. Avoid introducing bubbles. If bubbles are present after centrifugation, carefully aspirate to remove the bubbles first, prior to aspirating the body of the supernatant.
8. Wash organoids again to remove remaining freezing media. Add 5 mL of DMEM/F-12 washing solution, carefully resuspend the crypts using a p1000 tip and centrifuge the organoid suspension at 200 x g for 5 minutes at 4°C. Carefully remove and discard the supernatant.
9. Resuspend the organoids by adding 150 µL of room temperature (15-25°C) complete IntestiCult™ Organoid Growth Medium.
10. Add 150 µL of BME to the organoid suspension. Mix the suspension by pipetting up and down 5 to 10 times to ensure a consistent density and viscosity throughout the sample. Avoid introducing bubbles.
11. Using a pre-wetted tip, carefully pipette 50 µL of the medium/BME suspension into the center of each of 6 wells of a pre-heated 24-well plate to form domes. To prevent air bubbles when plating, dispense to the first stop of the pipette.

    Note: Proceed quickly to ensure BME does not polymerize before dome formation.
12. Without disrupting the domes, place lid on the culture plate and gently transfer it to the incubator for a 10-min incubation at 37°C, 5% CO_2. Ensure to transfer the plate very steadily without tipping or using swift movements.
13. Once the polymerization period is over, transfer the dome-containing plate back to the biological safety cabinet. Ensure BME domes have preserved their integrity and have not dispersed across the well.

14. Fill the dome-containing wells with 500 µL room temperature (15-25°C) complete IntestiCult™ Organoid Growth Medium by pipetting the medium gently down the sidewall of the well. Do not pipette the medium directly onto the domed cultures.
15. Add sterile PBS to all unused wells to ensure proper hydration of the cultures.
16. Place the lid on the culture plate and incubate at 37°C and 5% CO_2.
17. Exchange the culture medium 3 times per week by carefully aspirating the existing liquid medium, keeping the pipette tip at the edge of the well bottom. Replace with 500 µL fresh, room temperature (15-25°C) complete IntestiCult™ Organoid Growth Medium.
18. For the best results, passage the previously frozen organoids 2 times after thawing before beginning experiments. Organoid growth may be slow in the first passage after thawing. The organoids should be ready for passage at 7 to 14 days of culture after thawing, and 7 to 10 days after each passage.

The combination of these 4 steps allowed us to successfully culture normal colonic organoids derived from human patients and store them for an extended period, preserving their viability and functionality for further experiments in the future.

4.3.5 Serial human colonic organoids formation assay

Previously in the lab, we have treated primary CRC organoids from 5 independent patients with escalating doses of VXN resulting in significant reduced organoid counts and average sizes. For this experiment, the organoids formation assay, equal number of patient-derived CRC cells are seeded per well, as single-cells, and treated with VXN for 7 days with increasing doses of the drug (0.25 μM, 0.5 μM, and 1.0 μM). After the treatment is completed, the organoids are harvested and re-seeded as secondary organoids, now with no drug treatment. After 7 days, the plate is scanned, and the organoids formation, both size and number, are compared between control and treatments. VXN substantially blocked the capacity of dissociated primary organoid cells to initiate secondary organoid formation at doses as low as 0.25 μM (data not shown).

Once the patient-derived colonic organoids were established in the lab, the first experiment designed to test them was to reproduce the organoids formation assay. VXN had no significant effects on primary and secondary organoid formation from normal colonic crypts at 0.25 or 0.5 μM, and a small effect on organoid average size and count was observed at 1 μM (**Figure 18**).

Additionally, VXN has been tested in cell lines (HIEC versus HT29 and HCT116) and shown to be selective to cancer cells. Now, in our patient-derived organoids (normal versus CRC) the drug has shown much greater toxicity in CRC organoids than in normal colonic organoids. Therefore, this model has worked as a normal counterpart tool to study the toxicity of drugs.

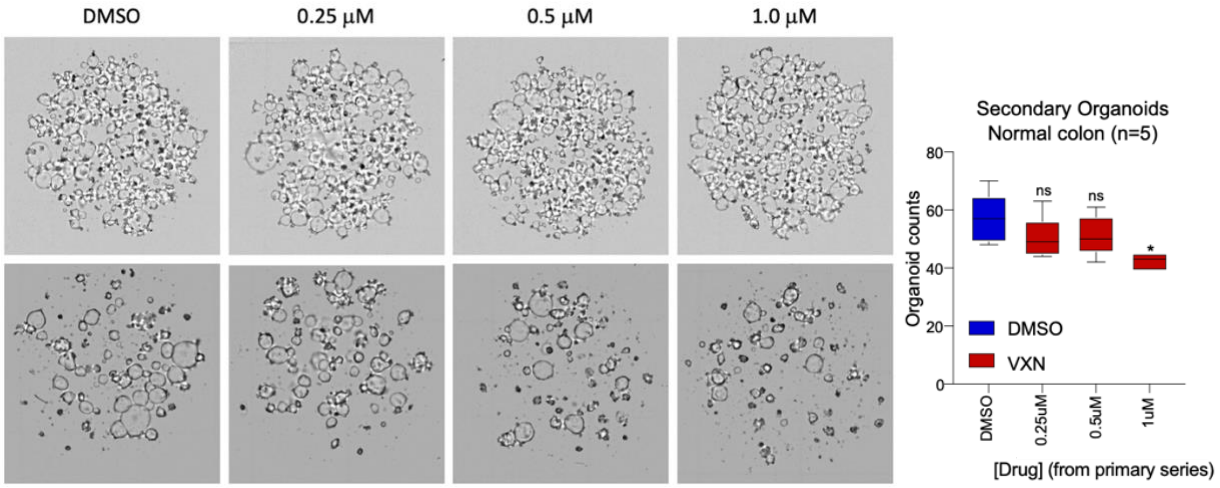

Figure 18 – **Serial human colonic organoids assay.** Representative whole-well brightfield imaging scans of primary (top row) and secondary (bottom row) patient-derived colonic organoids treated with VXN (7 days, 0.25 - 1 µM) vs DMSO (n=5).

To further test the applicability of colonic organoids in different settings, we tested them on a 3D bioprinter demo to see if we could seed 3D domes containing colonic organoids, where there are 3 technical replicates in each well, in a 24-well plate (**Figure 19A**).

Normal colonic organoids were also used for single-cell Western blot analysis. For that purpose, the following protocol has been used to seed cells from colonic crypts onto the single-cell Western blot chip:

4.3.6 Human colonic epithelia for single-cell Western blot protocol:

1. Gently aspirate the media from the well without disturbing the dome.
2. Add 200 μL of Cell Recovery Solution on top of the exposed dome in each well to chemically dissociate the BME domes and organoids. Incubate at room temperature (15-25ºC) for 1 minute.
3. Pre-wet a p1000 tip with Cell Recovery Solution and break up the dome and organoids by pipetting up and down approximately 10 times. Transfer the organoid suspension to a 1.5 mL tube and incubate on ice.
4. Every 5 minutes, invert the tube and place back on ice to prevent the gel settling at the bottom of the tube.
5. After 20 minutes on ice, centrifuge the sample at 400 x g for 5 minutes. If Matrigel has not fully dissolved, maintain on ice for further 5 minutes, and repeat until this is the case.
6. Remove supernatant and resuspend in 500 μL of pre-warmed TrypLE. Incubate for 10 to 25 minutes in a water bath at 37ºC.

Note: Check under the microscope 10 μL of the cell suspension to see if the dissociation was complete. If not, incubate the cells for an extra 5 minutes at 37ºC and check it again. Repeat that process until most of the sample consists of a single-cell suspension.

7. Add 500 μL of refrigerated DMEM + 1% BSA and centrifuge at 400 x g for 5 minutes. Remove the supernatant and resuspend in 500 μL of refrigerated DMEM + 1% BSA.
8. Centrifuge at 400 x g for 5 minutes. Remove the supernatant and resuspend in 1X Suspension buffer for single-cell Western blot.
9. Pre-coat a 50 mL conical tube with 1X Suspension buffer for single-cell Western blot. Pass the cell suspension through a 70 μm cell strainer, to eliminate remaining multicellular aggregates, to the pre-coated 50 mL conical tube.
10. Proceed with cell count and, in a new 1.5 mL microtube, prepare a single-cell suspension of 1 x 10^5 cells per mL in 1X Suspension buffer for single-cell Western blot.

    Note: If necessary, centrifuge the sample at 450 x g for 5 minutes at 4ºC. Discard the supernatant and resuspend the cells in 1 mL of 1X Suspension buffer for single-cell Western blot and count cells again. Keep cells on ice until they are used for the required experiment.

4.3.7 Application of human colonic organoids in drug screening pipeline

CRC organoids are a promising model to test cancer stem cells activity with several advantages compared to 2D-cell lines. They can be seeded in three-dimensional domes made of BME which resemble the structure and environment of the tumor, making them valuable tools for studying cancer and testing drugs. Notably, the recognized “gold standard” material for the BME

is the Matrigel, which is a basement membrane extract mostly composed of laminin and collagen IV [142].

The effects of drugs on organoids can be determined via techniques including immunostaining, gene expression analysis, clonogenic self-renewal assays, and single-cell proteomics. These methods can provide crucial information on cell viability, proliferation, multi-lineage reconstitution, differentiation state, tissue morphology, or expression of specific biomarkers determining whether a drug is effective. When performing experiments with organoids, maintaining proper controls is essential. For instance, drug-treated CRC tumor organoids should not only be compared with untreated CRC tumor organoids but also with their healthy colonic counterpart, the normal colonic organoids.

The development of CSC-targeting drugs constitutes a substantial challenge due to the importance of several molecular networks shared between neoplastic stemness and healthy pools of stem cells. Thus, phenotypic drug screening approaches are best suited to identify context-specific compounds that disrupt CSC functions while exerting minimal impact on healthy stem cells.

To screen drug libraries comprising hundreds of compounds and keep consistency through each well, 3D printing brings enhanced reproducibility with consistent size, shape, and cellular composition. It can also offer scalability, allowing for high-throughput screening of drug libraries. In our lab, we focus on the discovery of clinically approved drugs, to test their ability to inhibit the promotion of CCSC phenotype. Our group recently developed a serial 3D organoid formation assay to evaluate the potential of experimental compounds to block CSC functions *ex vivo* [141]. Such a method helped identify compounds altering epigenetic and pluripotency networks essential to human colorectal CSCs. Emerging 3D bioprinting technology enables miniaturization and

increased throughput of organoid formation assays measuring clonogenicity capacities in tissue samples [131, 143].

With this normal colonic organoid system, we will be able to strengthen our drug screening pipeline, using CRC organoids to screen for drugs and colonic organoids to assess selective toxicity of main hits (**Figure 19B**).

Using a temperature-controlled basement membrane extract bioprinter, we adapted our serial 3D organoid formation assay to perform rapid and cost-efficient drug screening experiments. For instance, using 24 and 96-well culture plates, we were able to print mini domes of basement membrane extract containing fragments of patient-derived colorectal tumors or healthy colonic epithelium. This system can be used to compare the efficacy of various chemical entities to block clonogenic functions in primary colorectal tumor organoids versus healthy colonic organoids. Such a bioprinting process is also valuable in generating miniaturized organoid cultures from human pluripotent stem cells and standard immortalized lines for screening purposes.

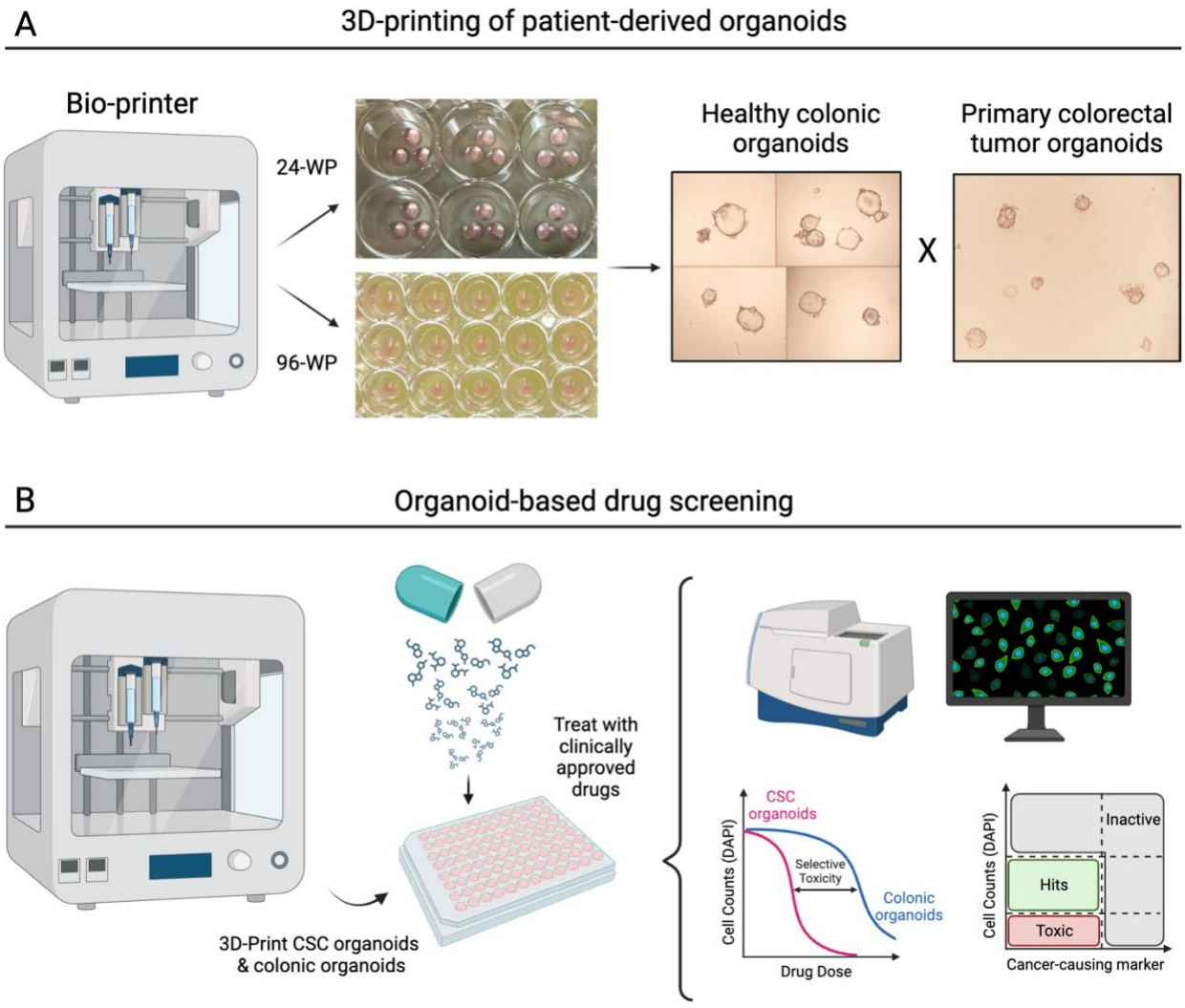

Figure 19 – **Applications for normal colon organoids. A)** 3D printing of human patient-derived colonic organoids. Bioprinter successfully seeded BME domes of 13 μL each in a 24-well plate. **B)** Representation of the high-throughput drug screening pipeline to identify repurposed drugs using 3D-printed organoids. Created with BioRender.com.

Discussion

6.1 Summary

Colorectal cancer treatment can be challenging, especially in the later stages of the disease. While great improvements have been made in the past decades, the combination of current therapies is still not efficient in eradicating the most advanced malignancies. The elevated activity of retrotransposable elements has been correlated with aggressive types of colorectal tumors. Therefore, targeting this aspect of tumorigenic cells could improve current pharmacological therapeutics.

The overall goal of my master's was to develop new tools to modulate retrotransposable element activity in colorectal cancer. Briefly, I have characterized the impact of a new clinically safe drug, Vanoxerine, previously identified in our lab as part of a phenotypic drug screening assay to screen repurposed compounds, on the reactivation of transposable elements and the stimulation of an innate antiviral response in CRC cells. This drug has been identified as a molecule capable of reduce CRC tumor growth and tumor-initiating capacity of colorectal cancer stem cells (data not shown), decrease DNA methylation and histone methylation levels, increase transposable elements activity followed by an induction on the immune response. Additionally, I have demonstrated an overall higher expression of L1ORF1p in cancer cell lines versus normal cell line and higher expression in tumor versus normal patient-derived tissues. The drug-induced global hypomethylation, by 5AZA, promotes the abundance of nuclear L1ORF1p, which is associated with LINE-1 retrotransposition events. Subsequently, I have introduced Ubrogepant and Dihydroergotamine as two drug candidates resulting from a virtual drug screening. These candidates target L1ORF1p as a means to prevent the nuclear translocation of ribonucleoprotein

particles and potentially downregulate retrotransposition levels in colorectal cancer. In the results presented in this thesis, these 2 compounds did not significantly decrease the levels of retrotransposition events, however, higher doses and longer treatments could demonstrate a significant effect. Other compounds from the drug screening, the remaining 9 molecules previously identified, could potentially demonstrate effects on retrotransposition levels in colorectal cancer.

To further investigate this goal, Objective 3 of my thesis focused on establishing a protocol that would allow the direct comparison of patient-derived CRC organoids with their respective patients' normal colonic organoids. This comparison serves as the gold standard for assessing the efficacy and toxicity of novel therapeutics *ex vivo*.

6.2 Objective 1: Characterization of a new clinically safe drug that activates transposable elements expression in colorectal cancer

Epigenetic modifications are tightly involved in tumorigenesis and aggressiveness of cancer cells. One of the consequences of a well-documented epigenetic modification in colorectal cancer, DNA methylation [130, 144], is the reactivation of retrotransposable elements upon LINE-1 hypomethylation [145]. Previously in our lab, we have demonstrated that the inhibition of G9a, a histone methyltransferase enzyme, not only significantly reduced tumor-initiating activity in patient-derived CRC stem cells, but also significantly reduced DNA methylation in L1ORF2 and 5'UTR regions of LINE-1 elements. This was accompanied by significant increases in LINE-1 transcripts, supporting the reactivation of such retrotransposable elements in response to DNA hypomethylation [131].

In the course of my master's, I have characterized the reactivation of retrotransposable elements, including LINE elements, upon treatments of colorectal cancer cells with VXN, a

compound discovered through a phenotypic high-throughput drug screening campaign executed in our lab, and which effectively decreases the levels of G9a expression in human CRC, consequently diminishing H3K9me2 deposition and stimulating TE activity. Corroborating the current literature, the reactivation of LINE-1 elements induces a viral mimicry state resulting in an increase on type-1 interferon response, a vital component of the intracellular antiviral defense response [107, 109, 110, 114].

Interestingly, a recent paper has been published reporting on the frequency of somatic retrotransposition of LINE-1 over a lifetime in healthy colonic epithelium and colorectal tumors [80]. Upon whole-genome sequencing analysis, colonic epithelium showed lower levels of DNA methylation compared to other cell types, accompanied with increases in LINE-1 mRNA levels, consistent with a role for DNA methylation in retrotransposon silencing [80]. Considering the tools available, in addition to those in progress, or proposed to target different stages of LINE1 retrotransposons lifecycle, it is still challenging to determine the precise impact of LINE1 reactivation in individuals with CRC. On one hand, LINE1s and other classes of TEs function as a driving force for CRC tumor progression, contributing to intratumor heterogeneity, and which should be blocked. On the other hand, LINE1 epigenetic de-repression and active transcription has been seen as valuable asset to be maintained and even harnessed as a safeguard promoting antitumor immune response in CRC patients. The best of both worlds should be considered by developing combination therapies targeting TE genomic integration while promoting their epigenetic de-repression and associated viral mimicry [96], which was approached in Objective 2.

To fully assess the reactivation of the immune response through RE-induced viral mimicry, *in vivo* studies were conducted to acquire a more realistic and comprehensive understanding of the intricate immune system and the tumor microenvironment. For this purpose, a murine syngeneic

model was employed. The introduction of MC38 cells into a C57BL/6 mouse model represents an MSI model, which is expected to resemble a subtype of colon cancer responsive to current immunotherapies. In contrast, the injection of CT26 cells into BALB/C mice signifies an MSS model, typically unresponsive to immunotherapies. Following the treatment of recipient mice harboring tumors, analyses involving immunohistochemistry, assessment of 10 distinct T cell markers expression by qPCR, and histopathological examination by a certified pathologist were performed on VXN-treated tumors in comparison to the vehicle control group. Regardless of the murine model, VXN treatment effectively elevated the percentage of CD8-positive cells per tumor, augmented lymphocyte infiltration, and induced an interferon response.

Ultimately, this suggests that G9a silencing exerted by VXN activates TE expression and restores an immune-responsive tumor microenvironment in CRC.

6.3 Objective 2: To develop new tools to downregulate TE mobility in colorectal cancer

LINE-1, as one of the main families of retrotransposons elements, holds significant importance as a target for studying TE mobility in human cells. L1ORF1p is recognized for its role in facilitating the nuclear translocation of LINE-1 ribonucleoprotein particles [146]. In addition, given the relevance of L1ORF1p as both chaperone and RNA binding protein throughout all the stages of retrotransposition, discovering novel high-affinity disruptors of L1ORF1p function would bring crucial insights into the impact of LINE-1 RT on cells and ways to modulate this process.

Notably, aberrant expression of L1ORF1p is suggested to be correlated with cancer progression and adverse prognosis [139, 147, 148] despite the fact that there is a significant lack of understanding regarding to the mechanisms that contribute to that up-regulation in tumors. DNA

hypomethylation is correlated to the increase of retrotransposable elements activity, as confirmed in Objective 1 and described in previous studies [50, 131]. The reactivation of LINE-1 retrotransposable elements due to the hypomethylation of the LINE-1 promoter (5'UTR), accompanied by the higher level of LINE-1 transcription, marking the progression of cancers, such as colorectal adenomas and adenocarcinomas, and chronic myeloid leukemia [149, 150]. In this study, consistent with previous research [139], L1ORF1p is found to be highly expressed in cancer cells, both *in vitro* and in patient-derived samples. Additionally, TE activity is induced by DNA demethylation, leading to increased expression and nuclear presence of L1ORF1p, suggesting an enhanced LINE-1 activity. This was further corroborated by the L1 reporter assay, revealing elevated retrotransposition levels following drug-induced DNA demethylation. Together, these results support that L1ORF1p expression and LINE-1 retrotransposition levels are significantly correlated with malignancy.

Given that currently there are no compounds targeting L1ORF1p to inhibit its functions in LINE-1 retrotransposition, literature research was performed to gather information for an *in silico* docking approach. The crystal structures of trimeric L1ORF1p and the NMR solution structures of its individual domains have revealed a sophisticated and intricately organized RNA-packaging protein that also possesses remarkable flexibility [121]. L1ORF1p displays a distinctive domain arrangement comprising an N-terminal coiled coil that leads to protein trimerization, a central RNA recognition motif (RMM) domain, and a C-terminal domain (CTD) [121, 151-153]. Both the RMM and CTD domains can selectively bind single-stranded RNA within the trimeric context, while slight mutations intended to disrupt its delicate structure resulting in the impairment of retrotransposition [121].

In light of the above, drug candidates were docked in the RMM-CTD domains of L1ORF1. Although the virtual docking displayed promising results, including low binding energy and multiple binding poses for each drug candidate, further investigation is still required to support this predictive computational binding between L1ORF1p and the drug candidates' molecules.

Interestingly, both drug candidates were revealed to not be toxic to both normal intestinal cells (HIEC) and cancer cells (HCT116, HT29 and HeLa) despite the high tested doses (10 μM). Furthermore, permeability prediction analysis demonstrated that both compounds can passively permeate through the cellular membrane. When tested in a cancer cell line, our results suggest that both compounds counteract the effects of 5AZA, encompassing aspects of nuclear translocation and protein expression of L1ORF1p. Preliminary data on LINE-1 retrotransposition levels, upon treatment with L1ORF1p inhibitor candidates could not support a potential inhibitory effect from these compounds on the frequency of LINE-1 insertions into the genome. It is possible that 5AZA treatments increase LINE-1 activity to a point where DHE and UBR effects on L1ORF1 are insufficient to markedly abrogate genomic insertion of reverse-transcribed elements. Additional validation of my findings in additional CRC models and further investigations on other drug candidates will be required in the future.

Taken together, these preliminary results have confirmed that LINE-1 activity is elevated in cancer cells. Moreover, an *in silico* drug screening for L1ORF1p disruptors has successfully identified drug candidates that modulate the protein levels and subcellular distribution of L1ORF1p in CRC cells. Further molecular biology studies will be necessary to confirm the direct interaction between DHE and UBR and L1ORF1p.

6.4 Objective 3: Establishment of colonic organoids derived from healthy tissues as a normal counterpart tool to study the toxicity of novel therapeutics

In the past few decades, the transition from growing two-dimensional cell cultures to three-dimensional cultures has brought an impactful shift in health sciences research. Organoids, a more specialized form of 3D culture, is an emerging technique that represents a significant advancement, offering a more sophisticated and intricate model compared to monolayer cellular cultures, which have the capacity to mimic the architectural structure and functional characteristics of organs [154]. The development of "gut-organoids" has facilitated the growth of normal crypt units that faithfully replicate numerous aspects of colonic physiology, potently bridging the gap between traditional cell cultures and intricate human tissues, thereby paving the way for exploring disease mechanisms, evaluating therapeutic interventions, and investigating cancer.

Upon researching multiple protocols online, troubleshooting, and making necessary improvements, I successfully established a culture method for normal human colonic organoids. This technique utilizes primary samples obtained from patients with colorectal cancer, which was made possible through collaboration with the Global Tissue Consenting program at The Ottawa Hospital. Specifically, patients who underwent tumor resection surgery provided both tumor tissue and surrounding normal tissue, for which I utilized the latter for the crypt isolation protocol.

The normal tissue adjacent to the tumor (NAT) is frequently used as a control in cancer research. Utilizing NAT as a normal control offers many advantages, including the relative convenient accessibility and the control for variability between individuals and anatomic regions. However, transcriptomic profiling studies have shown that NAT has morphologically normal but molecularly altered cells [155]. That being said, comparing patient-derived tumors and NAT tissues provides valuable insights for drug screening. This includes revealing cancer-selective drug

candidates, predicting drug efficacy and toxicity of compounds in tumor-derived cells versus normal colon-derived cells, and ultimately gathering information from a model that offers a greater complexity of human tissues than 2D cell culture. However, it is important to understand its limitations. Due to the differences between NAT and healthy normal tissues, potential therapeutic target candidates may be overlooked during drug screenings.

Through the dissociation of primary colon tissues and isolation of viable crypts, these patient-derived samples can be cultured under the same conditions and compared between treatments, based on discrepancies in the number, size, and shape of the resulting organoids. As observed in Objective 3, patient-derived colonic organoids were used to validate that specific drug candidates previously identified by our lab exerted limited impact on healthy colonic stem cell functions, despite having substantial inhibitory effects on CCSC functions.

The application of this technique proves to be highly valuable in cancer research, although some aspects of the culture process need to be considered, including the media. When preparing the media for organoid culture, the list of components can be quite extensive. Despite the advent of conditioned media that contain Wnt3a, Rspondin1, and Noggin [156], these media require fetal bovine serum, growth factors, which further adds potential variability and cost. One alternative is to use defined media with purified components (i.e., IntestiCult), which affects the costs of this system as well. Moreover, the use of a three-dimensional matrix (i.e., Matrigel) to support the organoid cultures, is an expensive and poorly defined heterogeneous protein mixture. In fact, cost, and unknown variables are important limitations to take into consideration when culturing organoids.

Other elements to take into consideration are some critical aspects of the crypt isolation protocol. The first passages are when most of the crypts die and only a few will survive the splitting

process. Hence, it is necessary to treat those organoids carefully and ensure that fresh media is provided every other day. Besides, not all patient-derived samples are capable of generating crypts that could be passaged and propagated. This phenomenon seems to be patient-dependent and is also directly correlated to the size and the freshness of the tissue sample delivered following surgical removal. Furthermore, it is also during the first couple of days of culturing isolated crypts the higher chances of bacterial and fungal contamination. Due to the source of the tissue sample, it is not surprising that bacterial contamination is very common, therefore is it mandatory the use of a combination of antibacterial and antifungal drugs, such as Penicillin and Streptomycin (PenStrep) and Amphotericin B.

The culture of normal colonic crypts as organoids in 3D domes provides them with the flexibility to allow for budding and formation of cyst-like structures that closely resemble the physiological aspects of colonic tissue. However, this approach could also present some challenges. For instance, passaging an equal number of organoids as crypts might prove difficult, as the splitting process tends to fragment large organoids into smaller ones in a non-homogenous manner. Additionally, automatic counting of colonic organoids using imaging software can pose challenges due to the lack of circularity in their structures.

Lastly, the described culturing method for colonic organoids does not consider the involvement of tumor microenvironment components, including stromal elements and immune cells, when studying tumor biology and drug responses. To address this limitation in *ex vivo* organoid systems, recent advancements have introduced co-culture techniques. These techniques could potentially be incorporated and adapted into this protocol to provide a more accurate representation of the tumor microenvironment. Furthermore, it's important to note that *ex vivo* drug treatments differ from *in vivo* administration, where crucial pharmacological factors like

pharmacokinetics and pharmacodynamics cannot be assessed. Nevertheless, this approach allows for a rapid and cost-effective evaluation of the impact of therapeutics on colorectal cancer stem cell activity within patient-derived tissues. This method has shown promise in predicting therapeutic outcomes when applied to preclinical *in vivo* serial tumor transplantation models [143].

Together, establishing a patient-derived healthy colon organoid protocol permitted us to successfully grow normal organoids from human CRC patients, propagate them, and create a biobank of patient-derived colon organoids for future experiments, such as drug screening and drug selectivity/toxicity assays.

Conclusion and Future Directions

Through the completion of this project, I have investigated the impact of specific drugs on retrotransposable elements activity in CRC and developed a tool for studying the level of toxicity of certain drugs in normal colonic epithelium tissues. Initially, I revealed the impact of a novel anti-CSC compound on transposable elements activation and its influence on triggering an innate antiviral response in colorectal cancer models. Furthermore, my work highlighted that LINE-1 activity is more pronounced in cancer cells compared to normal colonic crypt cells. Since the reactivation of retrotransposable elements is present in CRC and is only one of the hallmarks of this type of cancer contributing to the tumorigenesis and aggressiveness of the tumors, targeting L1ORF1p activity could hold promise for the treatment of CRC patients in combination with current therapies, preventing the progression of more invasive cases of this disease. Lastly, I established a protocol for culturing patient-derived healthy colon organoids, serving as a tool for drug screening, as well as conducting drug selectivity and toxicity assays.

However, numerous unresolved questions remain, presenting promising avenues for future research endeavors. The complete mechanism linking DNA hypomethylation to the reactivation of LINE-1 retrotransposition events remains insufficiently elucidated. Moreover, the events after reverse transcription implicated in the integration of LINE-1 into new genomic sites, such that multiple LINE-1 copies are truncated and unable to initiate and complete a retrotransposition cycle [82, 157]. Some proteins have been colocalized with LINE-1 RNAs within cytoplasmic stress granules, indicating that the confinement of LINE-1 RNAs into stress granules might be involved in breaking down or inhibiting the translation of these RNAs, although a deeper understanding of this mechanism requires further studies [158, 159]. Additionally, further analysis is warranted to

explore the impact on the viral mimicry when cells are treated with L1ORF1p inhibitors candidates. If the reinsertion of retrotransposable elements can be prevented while activating an immune response, inhibiting L1ORF1p could potentially offer a viable complementary therapeutic approach for colorectal cancer patients.

Future applications of patient-derived healthy colon organoids such as drug screening, using bioprinter to enhance reproducibility for organoids seeding, conducting secondary organoid assays to evaluate the effects of novel compounds on CSC activity, and more. Particularly, regarding the LINE-1 retrotransposition study, this system will be essential for assessing the influence of future L1ORF1 inhibitors on TE activity in normal colonic tissues and comparing the impact of these drugs on CRC organoids. Crucially, this study offers significant insights into LINE-1 activity in colorectal cancer and provides a tool for gauging the effects of targeting L1ORF1p on LINE-1 retrotransposition levels. Lastly, normal colonic organoids prove invaluable in research by facilitating the comparison of new compounds' toxicity and selectivity toward CRC cells *ex vivo*.

References

1. Society, C.C. *Colorectal cancer statistics*. 2022; Available from: https://cancer.ca/en/cancer-information/cancer-types/colorectal/statistics.
2. Akimoto, N., et al., *Rising incidence of early-onset colorectal cancer - a call to action.* Nat Rev Clin Oncol, 2021. **18**(4): p. 230-243.
3. Ishida, R., et al., *The Tissue-Reconstructing Ability of Colon CSCs Is Enhanced by FK506 and Suppressed by GSK3 Inhibition.* Mol Cancer Res, 2017. **15**(10): p. 1455-1466.
4. Amersi, F., M. Agustin, and C.Y. Ko, *Colorectal cancer: epidemiology, risk factors, and health services.* Clin Colon Rectal Surg, 2005. **18**(3): p. 133-40.
5. Muto, T., H.J. Bussey, and B.C. Morson, *The evolution of cancer of the colon and rectum.* Cancer, 1975. **36**(6): p. 2251-70.
6. Davies, R.J., R. Miller, and N. Coleman, *Colorectal cancer screening: prospects for molecular stool analysis.* Nat Rev Cancer, 2005. **5**(3): p. 199-209.
7. Kozuka, S., et al., *Premalignancy of the mucosal polyp in the large intestine: II. Estimation of the periods required for malignant transformation of mucosal polyps.* Dis Colon Rectum, 1975. **18**(6): p. 494-500.
8. Pino, M.S. and D.C. Chung, *The chromosomal instability pathway in colon cancer.* Gastroenterology, 2010. **138**(6): p. 2059-72.
9. Boland, C.R. and A. Goel, *Microsatellite instability in colorectal cancer.* Gastroenterology, 2010. **138**(6): p. 2073-2087 e3.
10. Toyota, M., et al., *CpG island methylator phenotype in colorectal cancer.* Proc Natl Acad Sci U S A, 1999. **96**(15): p. 8681-6.
11. Samowitz, W.S., et al., *Evaluation of a large, population-based sample supports a CpG island methylator phenotype in colon cancer.* Gastroenterology, 2005. **129**(3): p. 837-45.
12. Boland, C.R., N.L. Komarova, and A. Goel, *Chromosomal instability and cancer: not just one CINgle mechanism.* Gut, 2009. **58**(2): p. 163-4.
13. Wong, J.J., et al., *Methylation of the 3p22 region encompassing MLH1 is representative of the CpG island methylator phenotype in colorectal cancer.* Mod Pathol, 2011. **24**(3): p. 396-411.
14. Guinney, J., et al., *The consensus molecular subtypes of colorectal cancer.* Nat Med, 2015. **21**(11): p. 1350-6.
15. James D. Brierley, M.K.G., Christian Wittekind, *TNM Classification of Malignant Tumours*. 8th ed. 2016: Union for International Cancer Control (UICC). 272.
16. Society, C.C. *Treatments for colorectal cancer*. 2023; Available from: https://cancer.ca/en/cancer-information/cancer-types/colorectal/treatment/rectal-cancer.
17. Society, A.C. *Cancer Facts & Figures*. 2023; Available from: https://www.cancer.org/research/cancer-facts-statistics/all-cancer-facts-figures.html.
18. Brenner, H., M. Kloor, and C.P. Pox, *Colorectal cancer.* Lancet, 2014. **383**(9927): p. 1490-1502.

19. Darvin, P., et al., *Immune checkpoint inhibitors: recent progress and potential biomarkers.* Exp Mol Med, 2018. **50**(12): p. 1-11.
20. Le, D.T., et al., *Mismatch repair deficiency predicts response of solid tumors to PD-1 blockade.* Science, 2017. **357**(6349): p. 409-413.
21. van den Berg, I., et al., *Actual survival after resection of primary colorectal cancer: results from a prospective multicenter study.* World J Surg Oncol, 2021. **19**(1): p. 96.
22. Cho, Y.H., et al., *5-FU promotes stemness of colorectal cancer via p53-mediated WNT/beta-catenin pathway activation.* Nat Commun, 2020. **11**(1): p. 5321.
23. Miranda, A., et al., *Cancer stemness, intratumoral heterogeneity, and immune response across cancers.* Proc Natl Acad Sci U S A, 2019. **116**(18): p. 9020-9029.
24. Bayik, D. and J.D. Lathia, *Cancer stem cell-immune cell crosstalk in tumour progression.* Nat Rev Cancer, 2021. **21**(8): p. 526-536.
25. O'Brien, C.A., et al., *A human colon cancer cell capable of initiating tumour growth in immunodeficient mice.* Nature, 2007. **445**(7123): p. 106-10.
26. Suva, M.L., N. Riggi, and B.E. Bernstein, *Epigenetic reprogramming in cancer.* Science, 2013. **339**(6127): p. 1567-70.
27. de Sousa e Melo, F., et al., *A distinct role for Lgr5(+) stem cells in primary and metastatic colon cancer.* Nature, 2017. **543**(7647): p. 676-680.
28. Wainwright, E.N. and P. Scaffidi, *Epigenetics and Cancer Stem Cells: Unleashing, Hijacking, and Restricting Cellular Plasticity.* Trends Cancer, 2017. **3**(5): p. 372-386.
29. Plaks, V., N. Kong, and Z. Werb, *The cancer stem cell niche: how essential is the niche in regulating stemness of tumor cells?* Cell Stem Cell, 2015. **16**(3): p. 225-38.
30. Haebe, J.R., et al., *Emerging role of G9a in cancer stemness and promises as a therapeutic target.* Oncogenesis, 2021. **10**(11): p. 76.
31. Ben-Porath, I., et al., *An embryonic stem cell-like gene expression signature in poorly differentiated aggressive human tumors.* Nat Genet, 2008. **40**(5): p. 499-507.
32. Adorno-Cruz, V., et al., *Cancer stem cells: targeting the roots of cancer, seeds of metastasis, and sources of therapy resistance.* Cancer Res, 2015. **75**(6): p. 924-9.
33. Alvarez-Varela, A., et al., *Mex3a marks drug-tolerant persister colorectal cancer cells that mediate relapse after chemotherapy.* Nat Cancer, 2022. **3**(9): p. 1052-1070.
34. de Sousa, E.M.F. and F.J. de Sauvage, *Cellular Plasticity in Intestinal Homeostasis and Disease.* Cell Stem Cell, 2019. **24**(1): p. 54-64.
35. Widschwendter, M., et al., *Epigenetic stem cell signature in cancer.* Nat Genet, 2007. **39**(2): p. 157-8.
36. Miranda Furtado, C.L., et al., *Epidrugs: targeting epigenetic marks in cancer treatment.* Epigenetics, 2019. **14**(12): p. 1164-1176.
37. Park, J.W. and J.W. Han, *Targeting epigenetics for cancer therapy.* Arch Pharm Res, 2019. **42**(2): p. 159-170.
38. Bird, A., *Perceptions of epigenetics.* Nature, 2007. **447**(7143): p. 396-8.
39. Jones, P.A. and M.L. Gonzalgo, *Altered DNA methylation and genome instability: a new pathway to cancer?* Proc Natl Acad Sci U S A, 1997. **94**(6): p. 2103-5.
40. Chiang, P.K., et al., *S-Adenosylmethionine and methylation.* FASEB J, 1996. **10**(4): p. 471-80.

41. Yang, X., et al., *Targeting DNA methylation for epigenetic therapy.* Trends Pharmacol Sci, 2010. **31**(11): p. 536-46.
42. Feltus, F.A., et al., *DNA motifs associated with aberrant CpG island methylation.* Genomics, 2006. **87**(5): p. 572-9.
43. Bonazzi, V.F., D. Irwin, and N.K. Hayward, *Identification of candidate tumor suppressor genes inactivated by promoter methylation in melanoma.* Genes Chromosomes Cancer, 2009. **48**(1): p. 10-21.
44. Rodriguez, J., et al., *Chromosomal instability correlates with genome-wide DNA demethylation in human primary colorectal cancers.* Cancer Res, 2006. **66**(17): p. 8462-9468.
45. Hur, K., et al., *Hypomethylation of long interspersed nuclear element-1 (LINE-1) leads to activation of proto-oncogenes in human colorectal cancer metastasis.* Gut, 2014. **63**(4): p. 635-46.
46. Zouggar, A., J.R. Haebe, and Y.D. Benoit, *Intestinal Microbiota Influences DNA Methylome and Susceptibility to Colorectal Cancer.* Genes (Basel), 2020. **11**(7).
47. Cancer Genome Atlas Research, N., et al., *Genomic and epigenomic landscapes of adult de novo acute myeloid leukemia.* N Engl J Med, 2013. **368**(22): p. 2059-74.
48. Shlush, L.I., et al., *Identification of pre-leukaemic haematopoietic stem cells in acute leukaemia.* Nature, 2014. **506**(7488): p. 328-33.
49. Feinberg, A.P. and B. Vogelstein, *Alterations in DNA methylation in human colon neoplasia.* Semin Surg Oncol, 1987. **3**(3): p. 149-51.
50. Ehrlich, M., *DNA hypomethylation in cancer cells.* Epigenomics, 2009. **1**(2): p. 239-59.
51. Ogino, S., et al., *A cohort study of tumoral LINE-1 hypomethylation and prognosis in colon cancer.* J Natl Cancer Inst, 2008. **100**(23): p. 1734-8.
52. Antelo, M., et al., *A high degree of LINE-1 hypomethylation is a unique feature of early-onset colorectal cancer.* PLoS One, 2012. **7**(9): p. e45357.
53. Lander, E.S., et al., *Initial sequencing and analysis of the human genome.* Nature, 2001. **409**(6822): p. 860-921.
54. Hattori, M., et al., *L1 family of repetitive DNA sequences in primates may be derived from a sequence encoding a reverse transcriptase-related protein.* Nature, 1986. **321**(6070): p. 625-8.
55. Mouse Genome Sequencing, C., et al., *Initial sequencing and comparative analysis of the mouse genome.* Nature, 2002. **420**(6915): p. 520-62.
56. Swergold, G.D., *Identification, characterization, and cell specificity of a human LINE-1 promoter.* Mol Cell Biol, 1990. **10**(12): p. 6718-29.
57. Babushok, D.V. and H.H. Kazazian, Jr., *Progress in understanding the biology of the human mutagen LINE-1.* Hum Mutat, 2007. **28**(6): p. 527-39.
58. Kazazian, H.H., Jr., *Mobile elements: drivers of genome evolution.* Science, 2004. **303**(5664): p. 1626-32.
59. Martin, S.L., *The ORF1 protein encoded by LINE-1: structure and function during L1 retrotransposition.* J Biomed Biotechnol, 2006. **2006**(1): p. 45621.
60. Feng, Q., et al., *Human L1 retrotransposon encodes a conserved endonuclease required for retrotransposition.* Cell, 1996. **87**(5): p. 905-16.

61. Moran, J.V., et al., *High frequency retrotransposition in cultured mammalian cells.* Cell, 1996. **87**(5): p. 917-27.
62. Denli, A.M., et al., *Primate-specific ORF0 contributes to retrotransposon-mediated diversity.* Cell, 2015. **163**(3): p. 583-93.
63. Hohjoh, H. and M.F. Singer, *Sequence-specific single-strand RNA binding protein encoded by the human LINE-1 retrotransposon.* EMBO J, 1997. **16**(19): p. 6034-43.
64. Cost, G.J., et al., *Human L1 element target-primed reverse transcription in vitro.* EMBO J, 2002. **21**(21): p. 5899-910.
65. Wimmer, K., et al., *The NF1 gene contains hotspots for L1 endonuclease-dependent de novo insertion.* PLoS Genet, 2011. **7**(11): p. e1002371.
66. Beck, C.R., et al., *LINE-1 elements in structural variation and disease.* Annu Rev Genomics Hum Genet, 2011. **12**: p. 187-215.
67. Gilbert, N., et al., *Multiple fates of L1 retrotransposition intermediates in cultured human cells.* Mol Cell Biol, 2005. **25**(17): p. 7780-95.
68. Symer, D.E., et al., *Human l1 retrotransposition is associated with genetic instability in vivo.* Cell, 2002. **110**(3): p. 327-38.
69. Gilbert, N., S. Lutz-Prigge, and J.V. Moran, *Genomic deletions created upon LINE-1 retrotransposition.* Cell, 2002. **110**(3): p. 315-25.
70. Shi, X., A. Seluanov, and V. Gorbunova, *Cell divisions are required for L1 retrotransposition.* Mol Cell Biol, 2007. **27**(4): p. 1264-70.
71. Mita, P., et al., *LINE-1 protein localization and functional dynamics during the cell cycle.* Elife, 2018. **7**.
72. Xie, Y., et al., *Cell division promotes efficient retrotransposition in a stable L1 reporter cell line.* Mob DNA, 2013. **4**(1): p. 10.
73. Freeman, B.T., et al., *Identification of charged amino acids required for nuclear localization of human L1 ORF1 protein.* Mob DNA, 2019. **10**: p. 20.
74. Macia, A., et al., *Engineered LINE-1 retrotransposition in nondividing human neurons.* Genome Res, 2017. **27**(3): p. 335-348.
75. Kubo, S., et al., *L1 retrotransposition in nondividing and primary human somatic cells.* Proc Natl Acad Sci U S A, 2006. **103**(21): p. 8036-41.
76. de Boer, M., et al., *Primary immunodeficiency caused by an exonized retroposed gene copy inserted in the CYBB gene.* Hum Mutat, 2014. **35**(4): p. 486-96.
77. van den Hurk, J.A., et al., *L1 retrotransposition can occur early in human embryonic development.* Hum Mol Genet, 2007. **16**(13): p. 1587-92.
78. Kano, H., et al., *L1 retrotransposition occurs mainly in embryogenesis and creates somatic mosaicism.* Genes Dev, 2009. **23**(11): p. 1303-12.
79. Wissing, S., et al., *Reprogramming somatic cells into iPS cells activates LINE-1 retroelement mobility.* Hum Mol Genet, 2012. **21**(1): p. 208-18.
80. Nam, C.H., et al., *Widespread somatic L1 retrotransposition in normal colorectal epithelium.* Nature, 2023. **617**(7961): p. 540-547.
81. Szak, S.T., et al., *Molecular archeology of L1 insertions in the human genome.* Genome Biol, 2002. **3**(10): p. research0052.
82. Brouha, B., et al., *Hot L1s account for the bulk of retrotransposition in the human population.* Proc Natl Acad Sci U S A, 2003. **100**(9): p. 5280-5.

83. Sassaman, D.M., et al., *Many human L1 elements are capable of retrotransposition.* Nat Genet, 1997. **16**(1): p. 37-43.
84. Tubio, J.M.C., et al., *Mobile DNA in cancer. Extensive transduction of nonrepetitive DNA mediated by L1 retrotransposition in cancer genomes.* Science, 2014. **345**(6196): p. 1251343.
85. Iskow, R.C., et al., *Natural mutagenesis of human genomes by endogenous retrotransposons.* Cell, 2010. **141**(7): p. 1253-61.
86. Lee, E., et al., *Landscape of somatic retrotransposition in human cancers.* Science, 2012. **337**(6097): p. 967-71.
87. Shukla, R., et al., *Endogenous retrotransposition activates oncogenic pathways in hepatocellular carcinoma.* Cell, 2013. **153**(1): p. 101-11.
88. Ewing, A.D., et al., *Widespread somatic L1 retrotransposition occurs early during gastrointestinal cancer evolution.* Genome Res, 2015. **25**(10): p. 1536-45.
89. Doucet-O'Hare, T.T., et al., *LINE-1 expression and retrotransposition in Barrett's esophagus and esophageal carcinoma.* Proc Natl Acad Sci U S A, 2015. **112**(35): p. E4894-900.
90. Doucet-O'Hare, T.T., et al., *Somatically Acquired LINE-1 Insertions in Normal Esophagus Undergo Clonal Expansion in Esophageal Squamous Cell Carcinoma.* Hum Mutat, 2016. **37**(9): p. 942-54.
91. Bozic, I., et al., *Accumulation of driver and passenger mutations during tumor progression.* Proc Natl Acad Sci U S A, 2010. **107**(43): p. 18545-50.
92. Scott, E.C., et al., *A hot L1 retrotransposon evades somatic repression and initiates human colorectal cancer.* Genome Res, 2016. **26**(6): p. 745-55.
93. Miki, Y., et al., *Disruption of the APC gene by a retrotransposal insertion of L1 sequence in a colon cancer.* Cancer Res, 1992. **52**(3): p. 643-5.
94. Helman, E., et al., *Somatic retrotransposition in human cancer revealed by whole-genome and exome sequencing.* Genome Res, 2014. **24**(7): p. 1053-63.
95. Rodriguez-Martin, B., et al., *Pan-cancer analysis of whole genomes identifies driver rearrangements promoted by LINE-1 retrotransposition.* Nat Genet, 2020. **52**(3): p. 306-319.
96. Bergin, C.J.M.d.S., A.; Benoit, Y. D., *Where to Draw the LINE—Are Retrotransposable Elements Here to Stay?* Cancers, 2023. **15**(16): p. 4119.
97. Morrish, T.A., et al., *Endonuclease-independent LINE-1 retrotransposition at mammalian telomeres.* Nature, 2007. **446**(7132): p. 208-12.
98. Morrish, T.A., et al., *DNA repair mediated by endonuclease-independent LINE-1 retrotransposition.* Nat Genet, 2002. **31**(2): p. 159-65.
99. Belgnaoui, S.M., et al., *Human LINE-1 retrotransposon induces DNA damage and apoptosis in cancer cells.* Cancer Cell Int, 2006. **6**: p. 13.
100. Sinibaldi-Vallebona, P., et al., *A role for endogenous reverse transcriptase in tumorigenesis and as a target in differentiating cancer therapy.* Genes Chromosomes Cancer, 2006. **45**(1): p. 1-10.
101. Lindqvist, D., et al., *Oxidative stress, inflammation and treatment response in major depression.* Psychoneuroendocrinology, 2017. **76**: p. 197-205.

102. Teerawattanapong, N., et al., *Blood leukocyte LINE-1 hypomethylation and oxidative stress in knee osteoarthritis.* Heliyon, 2019. **5**(5): p. e01774.
103. Apostolou, P., et al., *Involvement of retrotransposon L1 in stemness and cellular plasticity.* Cell Commun Adhes, 2015. **22**(1): p. 1-7.
104. Khazina, E. and O. Weichenrieder, *Human LINE-1 retrotransposition requires a metastable coiled coil and a positively charged N-terminus in L1ORF1p.* Elife, 2018. **7**.
105. Fisher, M.D., *Irinotecan/5-FU/leucovorin, oxaliplatin/5-FU/leucovorin, and oxaliplatin/irinotecan are each effective in the treatment of 5-FU-resistant advanced colorectal cancer.* Clin Colorectal Cancer, 2001. **1**(2): p. 85-6.
106. Stresemann, C., et al., *Functional diversity of DNA methyltransferase inhibitors in human cancer cell lines.* Cancer Res, 2006. **66**(5): p. 2794-800.
107. Chen, R., C.A. Ishak, and D.D. De Carvalho, *Endogenous Retroelements and the Viral Mimicry Response in Cancer Therapy and Cellular Homeostasis.* Cancer Discov, 2021. **11**(11): p. 2707-2725.
108. Bannert, N., et al., *HERVs New Role in Cancer: From Accused Perpetrators to Cheerful Protectors.* Front Microbiol, 2018. **9**: p. 178.
109. Roulois, D., et al., *DNA-Demethylating Agents Target Colorectal Cancer Cells by Inducing Viral Mimicry by Endogenous Transcripts.* Cell, 2015. **162**(5): p. 961-73.
110. Chiappinelli, K.B., et al., *Inhibiting DNA Methylation Causes an Interferon Response in Cancer via dsRNA Including Endogenous Retroviruses.* Cell, 2017. **169**(2): p. 361.
111. Borden, E.C., *Interferons alpha and beta in cancer: therapeutic opportunities from new insights.* Nat Rev Drug Discov, 2019. **18**(3): p. 219-234.
112. Stone, M.L., et al., *Epigenetic therapy activates type I interferon signaling in murine ovarian cancer to reduce immunosuppression and tumor burden.* Proc Natl Acad Sci U S A, 2017. **114**(51): p. E10981-E10990.
113. Sheng, W., et al., *LSD1 Ablation Stimulates Anti-tumor Immunity and Enables Checkpoint Blockade.* Cell, 2018. **174**(3): p. 549-563 e19.
114. Lindholm, H.T., R. Chen, and D.D. De Carvalho, *Endogenous retroelements as alarms for disruptions to cellular homeostasis.* Trends Cancer, 2023. **9**(1): p. 55-68.
115. Chuong, E.B., N.C. Elde, and C. Feschotte, *Regulatory evolution of innate immunity through co-option of endogenous retroviruses.* Science, 2016. **351**(6277): p. 1083-7.
116. Zhang, S.M., et al., *KDM5B promotes immune evasion by recruiting SETDB1 to silence retroelements.* Nature, 2021. **598**(7882): p. 682-687.
117. De Cecco, M., et al., *L1 drives IFN in senescent cells and promotes age-associated inflammation.* Nature, 2019. **566**(7742): p. 73-78.
118. Banuelos-Sanchez, G., et al., *Synthesis and Characterization of Specific Reverse Transcriptase Inhibitors for Mammalian LINE-1 Retrotransposons.* Cell Chem Biol, 2019. **26**(8): p. 1095-1109 e14.
119. Baldwin, E.T., et al., *Human endogenous retrovirus-K (HERV-K) reverse transcriptase (RT) structure and biochemistry reveals remarkable similarities to HIV-1 RT and opportunities for HERV-K-specific inhibition.* Proc Natl Acad Sci U S A, 2022. **119**(27): p. e2200260119.
120. Lim, J., et al., *Extrahepatic carcinogenicity of oral nucleos(t)ide analogues in chronic hepatitis B carriers: A 35,000-Korean outcome study.* J Viral Hepat, 2022. **29**(9): p. 756-764.

121. Khazina, E., et al., *Trimeric structure and flexibility of the L1ORF1 protein in human L1 retrotransposition.* Nat Struct Mol Biol, 2011. **18**(9): p. 1006-14.
122. Dallakyan, S. and A.J. Olson, *Small-molecule library screening by docking with PyRx.* Methods Mol Biol, 2015. **1263**: p. 243-50.
123. Gaillard, T., *Evaluation of AutoDock and AutoDock Vina on the CASF-2013 Benchmark.* J Chem Inf Model, 2018. **58**(8): p. 1697-1706.
124. Trott, O. and A.J. Olson, *AutoDock Vina: improving the speed and accuracy of docking with a new scoring function, efficient optimization, and multithreading.* J Comput Chem, 2010. **31**(2): p. 455-61.
125. Forli, S., et al., *Computational protein-ligand docking and virtual drug screening with the AutoDock suite.* Nat Protoc, 2016. **11**(5): p. 905-19.
126. Laskowski, R.A. and M.B. Swindells, *LigPlot+: multiple ligand-protein interaction diagrams for drug discovery.* J Chem Inf Model, 2011. **51**(10): p. 2778-86.
127. Patro, R., et al., *Salmon provides fast and bias-aware quantification of transcript expression.* Nat Methods, 2017. **14**(4): p. 417-419.
128. Jin, Y. and M. Hammell, *Analysis of RNA-Seq Data Using TEtranscripts.* Methods Mol Biol, 2018. **1751**: p. 153-167.
129. Subramanian, A., et al., *Gene set enrichment analysis: a knowledge-based approach for interpreting genome-wide expression profiles.* Proc Natl Acad Sci U S A, 2005. **102**(43): p. 15545-50.
130. Baylin, S.B. and P.A. Jones, *A decade of exploring the cancer epigenome - biological and translational implications.* Nat Rev Cancer, 2011. **11**(10): p. 726-34.
131. Bergin, C.J., et al., *G9a controls pluripotent-like identity and tumor-initiating function in human colorectal cancer.* Oncogene, 2021. **40**(6): p. 1191-1202.
132. Benoit, Y.D., et al., *Sam68 Allows Selective Targeting of Human Cancer Stem Cells.* Cell Chem Biol, 2017. **24**(7): p. 833-844 e9.
133. Benoit, Y.D., et al., *Targeting SUMOylation dependency in human cancer stem cells through a unique SAE2 motif revealed by chemical genomics.* Cell Chem Biol, 2021. **28**(10): p. 1394-1406 e10.
134. Werbowetski-Ogilvie, T.E., et al., *Characterization of human embryonic stem cells with features of neoplastic progression.* Nat Biotechnol, 2009. **27**(1): p. 91-7.
135. Sachlos, E., et al., *Identification of drugs including a dopamine receptor antagonist that selectively target cancer stem cells.* Cell, 2012. **149**(6): p. 1284-97.
136. Baell, J.B. and G.A. Holloway, *New substructure filters for removal of pan assay interference compounds (PAINS) from screening libraries and for their exclusion in bioassays.* J Med Chem, 2010. **53**(7): p. 2719-40.
137. Moore, E., et al., *Characterization of Ubrogepant: A Potent and Selective Antagonist of the Human Calcitonin Gene–Related Peptide Receptor.* J Pharmacol Exp Ther, 2020.
138. Lesage, A.S., et al., *Agonistic properties of alniditan, sumatriptan and dihydroergotamine on human 5-HT1B and 5-HT1D receptors expressed in various mammalian cell lines.* Br J Pharmacol, 1998. **123**(8): p. 1655-65.
139. Chen, L., et al., *Prognostic value of LINE-1 retrotransposon expression and its subcellular localization in breast cancer.* Breast Cancer Res Treat, 2012. **136**(1): p. 129-42.
140. Hofer, M. and M.P. Lutolf, *Engineering organoids.* Nat Rev Mater, 2021. **6**(5): p. 402-420.

141. Bergin, C.J. and Y.D. Benoit, *Protocol for serial organoid formation assay using primary colorectal cancer tissues to evaluate cancer stem cell activity.* STAR Protoc, 2022. **3**(1): p. 101218.
142. Kleinman, H.K. and G.R. Martin, *Matrigel: basement membrane matrix with biological activity.* Semin Cancer Biol, 2005. **15**(5): p. 378-86.
143. Masibag, A.N., et al., *Pharmacological targeting of Sam68 functions in colorectal cancer stem cells.* iScience, 2021. **24**(12): p. 103442.
144. Ehrlich, M., *DNA methylation in cancer: too much, but also too little.* Oncogene, 2002. **21**(35): p. 5400-13.
145. Lam, K., et al., *DNA methylation based biomarkers in colorectal cancer: A systematic review.* Biochim Biophys Acta, 2016. **1866**(1): p. 106-20.
146. Doucet, A.J., et al., *Characterization of LINE-1 ribonucleoprotein particles.* PLoS Genet, 2010. **6**(10).
147. Whongsiri, P., et al., *LINE-1 ORF1 Protein Is Up-regulated by Reactive Oxygen Species and Associated with Bladder Urothelial Carcinoma Progression.* Cancer Genomics Proteomics, 2018. **15**(2): p. 143-151.
148. Ardeljan, D., et al., *The Human Long Interspersed Element-1 Retrotransposon: An Emerging Biomarker of Neoplasia.* Clin Chem, 2017. **63**(4): p. 816-822.
149. Roman-Gomez, J., et al., *Promoter hypomethylation of the LINE-1 retrotransposable elements activates sense/antisense transcription and marks the progression of chronic myeloid leukemia.* Oncogene, 2005. **24**(48): p. 7213-23.
150. Shademan, M., et al., *Promoter methylation, transcription, and retrotransposition of LINE-1 in colorectal adenomas and adenocarcinomas.* Cancer Cell Int, 2020. **20**: p. 426.
151. Basame, S., et al., *Spatial assembly and RNA binding stoichiometry of a LINE-1 protein essential for retrotransposition.* J Mol Biol, 2006. **357**(2): p. 351-7.
152. Martin, S.L., et al., *Trimeric structure for an essential protein in L1 retrotransposition.* Proc Natl Acad Sci U S A, 2003. **100**(24): p. 13815-20.
153. Khazina, E. and O. Weichenrieder, *Non-LTR retrotransposons encode noncanonical RRM domains in their first open reading frame.* Proc Natl Acad Sci U S A, 2009. **106**(3): p. 731-6.
154. Almeqdadi, M., et al., *Gut organoids: mini-tissues in culture to study intestinal physiology and disease.* Am J Physiol Cell Physiol, 2019. **317**(3): p. C405-C419.
155. Aran, D., et al., *Comprehensive analysis of normal adjacent to tumor transcriptomes.* Nat Commun, 2017. **8**(1): p. 1077.
156. Miyoshi, H. and T.S. Stappenbeck, *In vitro expansion and genetic modification of gastrointestinal stem cells in spheroid culture.* Nat Protoc, 2013. **8**(12): p. 2471-82.
157. Perepelitsa-Belancio, V. and P. Deininger, *RNA truncation by premature polyadenylation attenuates human mobile element activity.* Nat Genet, 2003. **35**(4): p. 363-6.
158. Hu, S., et al., *SAMHD1 Inhibits LINE-1 Retrotransposition by Promoting Stress Granule Formation.* PLoS Genet, 2015. **11**(7): p. e1005367.
159. Goodier, J.L., et al., *LINE-1 ORF1 protein localizes in stress granules with other RNA-binding proteins, including components of RNA interference RNA-induced silencing complex.* Mol Cell Biol, 2007. **27**(18): p. 6469-83.

Appendix

Table 1. List of primers used for the RT-qPCR.

Oligonucleotides		
GAPDH Human	Forward	GAA ATC CCA TCA CCA ATC TTC CAG G
	Reverse	GCA ATT GAG CCC CAG CCT TCT C
IFIT1 Human	Forward	GCC TTG CTG AAG TGT GGA GGA A
	Reverse	ATC CAG GCG ATA GGC AGA GAT C
ISG15 Human	Forward	CTC TGA GCA TCC TGG TGA GGA A
	Reverse	AAG GTC AGC CAG AAC AGG TCG T
MX1 Human	Forward	GGC TGT TTA CCA GAC TCC GAC A
	Reverse	CAC AAA GCC TGG CAG CTC TCT A
IFI27 Human	Forward	CGT CCT CCA TAG CAG CCA AGA T
	Reverse	ACC CAA TGG AGC CCA GGA TGA A
OAS3 Human	Forward	CCT GAT TCT GCT GGT GAA GCA C
	Reverse	TCC CAG GCA AAG ATG GTG AGG A
Il12b Mouse	Forward	TTG AAC TGG CGT TGG AAG CAC G
	Reverse	CCA CCT GTG AGT TCT TCA AAG GC
Il4ra Mouse	Forward	ACC AGA TGG AAC TGT GGG CTG A
	Reverse	AGC AGC CAT TCG TCG GAC ACA T
Il7r Mouse	Forward	CAC AGC CAG TTG GAA GTG GAT G
	Reverse	GGC ATT TCA CTC GTA AAA GAG CC
Cd74 Mouse	Forward	GCT GGA TGA AGC AGT GGC TCT T
	Reverse	GAT GTG GCT GAC TTC TTC CTG G
Cd83 Mouse	Forward	ACC GTG GTT CTG AAG GTG ACA G
	Reverse	CCA GAG AGA AGA GCA ACA CAG C
Cd86 Mouse	Forward	ACG TAT TGG AAG GAG ATT ACA GCT
	Reverse	TCT GTC AGC GTT ACT ATC CCG C
Lcam1	Forward	AAA CCA GAC CCT GGA ACT GCA C

Mouse	Reverse	GCC TGG CAT TTC AGA GTC TGC T
Slamf6	Forward	CAG AGC CAA GAA TGC TGT CAG C
Mouse	Reverse	ACC ATA CTG CAT TCC AGG GTG G
Stap1	Forward	GAG CCA GTA CAA GAC TAT GCG G
Mouse	Reverse	AGT TTT TGC TGT CAC TAC CAG GC
Ccr7	Forward	AGA GGC TCA AGA CCA TGA CGG A
Mouse	Reverse	TCC AGG ACT TGG CTT CGC TGT A
GAPDH	Forward	GAT GCC CCC ATG TTT GTG AT
Mouse	Reverse	GGT CAT GAG CCC TTC CAC AAT

Table 2. List of antibodies and staining reagents.

Reagent	Dilution	Source	Identifier
Anti-Actin Monoclonal Ab	1:80,000 WB	Millipore	MAB1501
Human Anti-L1ORF1 Monoclonal Ab	1:1,000 WB 1:300 IF	Millipore	MABC1152
Hoechst 33342	1:1,000 IF	Invitrogen	H3570
Phalloidin CruzFluor™ 647	1:1,000 IF	Santa Cruz	sc-363797
Anti-Mouse IgG Alexa Fluor™ 488 Ab	1:500 IF	Invitrogen	A11001
Anti-Mouse IgG Alexa Fluor™ 647 Ab	1:500 IF	Invitrogen	A21235
Anti-Rabbit IgG Alexa Fluor™ 488 Ab	1:500 IF	Invitrogen	A11034
Anti-Rabbit IgG Alexa Fluor™ 647 Ab	1:500 IF	Invitrogen	A21443
Anti-Mouse IgG HRP-linked Ab	1:2,000 IF	Cell Signaling	7076S
Anti-Rabbit IgG HRP-linked Ab	1:2,000 IF	Cell Signaling	7074S
Anti-5-methylcytosine Ab	1:5,000 IF	Millipore	MABE146
Anti-OCT4A Ab	1:500 IF	Cell Signaling	C30A3
Anti-E-Cadherin Ab	1:250 IF	Cell Signaling	24E10
Anti-Histone H3 (di methyl K9) Ab	1:2,000 WB 1:500 IF	Abcam	ab1220
Anti-Histone H3 (tri methyl K9) Ab	1:3,000 WB	Abcam	ab8898
Anti-Histone H3 (tri methyl K27) Ab	1:1000 WB	Invitrogen	PA5-31817
Anti-Histone H3 Ab	1:100,000 WB	Abcam	ab1791
Anti-CD8 Ab	1:500 IF	Novus Biolog.	NBP1-49045

Table 3. List of cell lines and mouse strain used in this study.

Reagent	Source	Identifier
HIEC	ATCC	CRL-3266
SW480	ATCC	CCL-228
HT29	ATCC	HTB-38
HCT116	ATCC	CCL-247
293-FT	Thermo Fisher Scientific	R70007
MC38	Kerafast	ENH204-FP
C57BL/6 female mice	Charles River	Strain code: 027
HeLa	A gift from Dr. John Copeland, University of Ottawa	
t-hESC	A gift from Dr. Mickie Bhatia, McMaster University (Werbowetski-Ogilvie et al., 2009)	

Table 4. List of chemicals, reagents, and commercial assays.

Reagent	Source	Identifier
Dimethylsulfoxide (DMSO)	ATCC	CA95040-114L
Matrigel Matrix	Corning	354277
Cell Recovery Solution	Corning	354253
Gentle Cell Dissociation Reagent	Stem Cell Technol.	100-1077
Fetal Bovine Serum	Wisent Bioproducts	080-450
FBS Premium Quality	Wisent Bioproducts	080-450
KnockOut Serum Replacement	Gibco	10828028
Polybrene Transfection Reagent	Millipore Sigma	TR-1003-G
Lipofectamine LTX Reagent	Invitrogen	15338500
McCoy's 5A Medium w/ L-Gln and HEPES	Lonza	12-168F
OptiMEM reduced media	Gibco	31985-070
DMEM 1X	Wisent Bioproducts	319-005-CL
DMEM/F-12	Gibco	11-320-033
KnockOut DMEM	Gibco	10829018
Human Epithelium Growth Factor (hEGF)	Wisent Bioproducts	511-110-EU
HEPES buffer	Gibco	15630-080
GlutaMAX supplement	Gibco	35050-061
Collagenase Type IV	Stem Cell Technol.	07909
1X TrypLE Express Enzyme	Thermo Fisher	12605-010
Trypan Blue Stain	Thermo Fisher	T10282
Total RNA Purification kit	Norgen BIOTEK	37500
Power-up Syber Green Master mix	Thermo Fisher	A25742
SuperScript VILO cDNA Synthesis Kit	Invitrogen	11754050
Immobilon™ Forte Western HRP substrate	Millipore	WBLUF
BD Cytofix/Cytoperm kit	BD Bioscience	554714
QIAprep Spin Miniprep Kit	Qiagen	27104
VectaShield Antifade Mounting with DAPI	VectaShield	H-1200
ProLong Diamond Antifade Mounting with DAPI	Thermo Fisher	P36962

Formaldehyde	Millipore	47608
Triton X-100	Thermo Fisher	BP151-100
Tween-20	Thermo Fisher	BP337-500
Amersham ECL Full-Range Rainbow Ladder	VWR	CA95044-114L
HBSS	Gibco	14170-120
Nevirapine	Cayman	15117
Zidovudine	Cayman	15492
Ubrogepant	Adooq Bioscience	A21670
Dihydroergotamine	Tocris Bioscience	0475

Table 5. List of plasmid constructs used in this study.

Plasmid	Source	Identifier
pPAX.2	Addgene	12260
pMD2.G	Addgene	12259
pLKO.1 TRC	Addgene	10878
LINE-1 reporter	A gift from Dr. Derrick Gibbings, University of Ottawa	